




OPEN ACCESS

Original research

# High-affinity neoantigens correlate with better prognosis and trigger potent antihepatocellular carcinoma (HCC) activity by activating CD39<sup>+</sup>CD8<sup>+</sup> T cells

Ting Liu,<sup>1</sup> Jizhou Tan,<sup>1</sup> Minhao Wu,<sup>2</sup> Wenzhe Fan,<sup>1</sup> Jialiang Wei,<sup>1</sup> Bowen Zhu,<sup>1</sup> Jian Guo,<sup>1</sup> Shutong Wang,<sup>1</sup> Penghui Zhou,<sup>3</sup> Hui Zhang,<sup>2</sup> Liangrong Shi,<sup>4</sup> Jiaping Li <sup>1</sup>

► Additional material is published online only. To view, please visit the journal online (<http://dx.doi.org/10.1136/gutjnl-2020-322196>).

<sup>1</sup>Department of Interventional Oncology, The First Affiliated Hospital, Sun Yat-Sen University, Guangzhou, Guangdong, China

<sup>2</sup>Department of Immunology, Zhongshan School of Medicine, Sun Yat-sen University, Guangzhou, China

<sup>3</sup>State Key Laboratory of Oncology in South China, Collaborative Innovation Center for Cancer Medicine, Sun Yat-sen University Cancer Center, Guangzhou, China

<sup>4</sup>Radiological Intervention Center, Department of Radiology, Xiangya Hospital, Central South University, Changsha, Hunan, China

## Correspondence to

Dr Jiaping Li;  
[lijiap@mail.sysu.edu.cn](mailto:lijiap@mail.sysu.edu.cn)

TL, JT and MW contributed equally.

Received 12 June 2020  
Revised 3 November 2020  
Accepted 4 November 2020  
Published Online First  
1 December 2020



© Author(s) (or their employer(s)) 2021. Re-use permitted under CC BY-NC. No commercial re-use. See rights and permissions. Published by BMJ.

**To cite:** Liu T, Tan J, Wu M, et al. *Gut* 2021;**70**:1965–1977.

## ABSTRACT

**Objective** It remains controversial whether tumour mutational burden (TMB) or neoantigens are prognostic markers in hepatocellular carcinoma (HCC). This study aimed to define the function of TMB or neoantigens in antitumour immunotherapy.

**Design** Neoantigens of patients (n=56) were analysed by pVAC tools with major histocompatibility complex-1 (MHC-I) algorithms based on whole exome sequencing and neoantigens with mutant type IC<sub>50</sub> <50 nM were defined as high-affinity neoantigens (HANs). Patients were segregated into HAN-high/low groups by median of HAN value, and overall survival (OS) was analysed. Autologous organoid killing model was developed to clarify the antitumour activity of HANs.

**Results** The value of HAN showed a better correlation with OS ( $p=0.0199$ ) than TMB ( $p=0.7505$ ) or neoantigens ( $p=0.2297$ ) in patients with HCC and positively correlated with the frequency of CD39<sup>+</sup>CD8<sup>+</sup> tumour infiltrating lymphocytes (TILs). Furthermore, HAN-specific CD8<sup>+</sup> T cells were identified in CD39<sup>+</sup>CD8<sup>+</sup> TILs, which showed better antitumour activity in HAN-high versus HAN-low group. In addition, more effective HAN peptides were identified in HAN-high versus HAN-low group. Besides, flow cytometry data showed that in fresh tumour, CD39<sup>+</sup>PD-1<sup>int</sup>CD8<sup>+</sup> TILs displayed an effector phenotype and stronger antitumour activity in HAN-high versus HAN-low group. More importantly, patients in HAN-high versus HAN-low group showed a better prognosis after anti-PD-1 therapy.

**Conclusions** Our study first demonstrates that HAN value positively correlates with better OS in patients with HCC. HANs trigger antitumour activity by activating tumour-reactive CD39<sup>+</sup>CD8<sup>+</sup> T cells, and patients in HAN-high group benefited more from anti-PD-1 therapy than HAN-low group. These findings may provide a novel strategy for personalised antitumour therapies for HCC.

## INTRODUCTION

Hepatocellular carcinoma (HCC) accounts for nearly 90% of primary cancers and malignant tumours of the liver and is the second leading cause of death worldwide.<sup>1</sup> At present, there has been no satisfactory effective indicators for prognosis

## Significance of this study

### What is already known on this subject?

- Neoantigens are products of somatic non-synonymous mutations of tumour gene, which can be presented by antigen-presenting cells to elicit antigen-specific T cell response.
- It remains controversial whether neoantigens could be implied as the predictive marker of efficacy of prognosis in hepatocellular carcinoma (HCC).
- CD39 is a novel biomarker to distinguish tumour-specific CD8<sup>+</sup> T cells from bystander CD8<sup>+</sup> T cells.

### What are the new findings?

- The value of high-affinity neoantigen (HAN), but not tumour mutational burden or neoantigen, correlated with better overall survival and the frequency of CD39<sup>+</sup>CD8<sup>+</sup> tumour infiltrating lymphocytes (TILs) in HCC.
- HAN-specific CD8<sup>+</sup> T cells were identified in CD39<sup>+</sup>CD8<sup>+</sup> TILs, which showed better antitumour activity in HAN-high versus HAN-low group, and more effective HAN peptides were identified in HAN-high group.
- CD39<sup>+</sup>PD-1<sup>int</sup>CD8<sup>+</sup> TILs displayed an effector T cell phenotype and stronger antitumour activity in HAN-high versus HAN-low group.
- Patients in HAN-high versus HAN-low group showed a better clinical outcome after anti-PD-1 therapy.

### How might it impact on clinical practice in the foreseeable future?

- The identification of HANs responsible for personalised antitumour therapies and characterisation of their role in this process may help us to elucidate mechanisms of rejection and to identify prognostic markers and screen suitable patients with HCC for anti-PD-1 therapy.

of HCC treatment. Recently, tumour mutational burden (TMB) is considered as a biomarker to predict the therapeutic effect of prognosis in some

cancers.<sup>2,3</sup> However, the value of TMB is low in patients with HCC, and no significant correlation has been found between TMB and prognosis.<sup>4-6</sup> Therefore, the predictive value of TMB in HCC is uncertain.

Neoantigens are products of somatic non-synonymous mutations of tumour genes, which can be recognised and presented by antigen-presenting cells (APCs) to elicit antigen-specific T cell response.<sup>7</sup> Based on Whole exon sequencing (WES), prediction algorithms for major histocompatibility complex-1 (MHC-I) peptide binding affinity have been used to filter out thousands of personalised neoantigens for individual patients.<sup>8</sup> However, only a few of candidate neoantigens can efficiently activate T cell anti-tumour immune response. Therefore, some studies focused on improving the neoantigen screening so as to narrow the scope. For example, Rosenberg *et al* identified top 2% of epitopes that comprise peptides with high binding affinity in 10 patients with gastrointestinal tumours.<sup>9</sup> On this basis, some studies reported that patients can reacquire substantial complete response by injection of the candidate high MHC-I binding affinity neoantigen-loaded dendritic cells (DC) peptides in metastatic thymoma.<sup>10</sup> In addition, transfer of candidate neoantigen-activated specific autologous T cells has shown impressive efficiency in achieving the durable regression of metastatic breast cancer, colon cancer, bile duct cancer and so on.<sup>9,11,12</sup> However, whether high-affinity neoantigens (HANs) could trigger antitumour activity of patients with HCC remains unknown.

CD8<sup>+</sup> T cells plays an important role of specifically recognising and killing tumour cells via releasing cytotoxic molecules in anti-tumour immune response, whereas only part of CD8<sup>+</sup> tumour infiltrating lymphocytes (TILs) can recognise tumour-specific neoantigen and achieve targeted killing. Recently, increasing evidence has shown that CD39 is a marker of tumour-specific T cells,<sup>13-15</sup> though it was considered to be a biomarker of exhausted T cells in some studies. They found that CD39<sup>+</sup>CD8<sup>+</sup> T cells had stronger antitumour ability than CD39<sup>-</sup>CD8<sup>+</sup> T cells in six different malignant tumour types.<sup>14</sup> CD39 was identified as a biomarker to distinguish tumour-specific CD8<sup>+</sup> T cells from bystander CD8<sup>+</sup> T cells.<sup>16</sup> However, whether CD39 is associated with neoantigen-specific CD8<sup>+</sup> T cells that mediate antitumour immune response in the HCC needs to be studied.

Here, we found that the value of HAN showed a stronger correlation with better overall survival (OS) than TMB or neoantigens did in patients with HCC, and it was positively correlated with the frequency of CD39<sup>+</sup>CD8<sup>+</sup> TILs. More tumour-specific peptides were identified in HAN-high group than those in HAN-low group, which could activate tumour-reactive CD39<sup>+</sup>CD8<sup>+</sup> T cells. Therefore, our study revealed the antitumour activity of HANs in patients with HCC, providing new insights regarding prognosis prediction and personalised HAN immunotherapy in HCC.

## MATERIALS AND METHODS

From 2017 to 2020, needle biopsies and blood samplings were taken from a cohort of 56 patients with HCC in The First Affiliated Hospital of Sun Yat-sen University. No treatment was taken when needle biopsies was collected. The detailed patients' data including future treatments were shown in online supplemental table 1). The project was approved with the patient's informed consent and ethical approval (2018 [43]).

### WES-sequence and neoantigen identification

Collected tumour and blood samples were sent to GenomiCare Biotechnology (Shanghai), Shanghai 201210, China for targeted

next generation sequencing analysis. The exome DNA was captured using the SureSelect Human All Exon V7 kit (#5991-9039EN Agilent USA), prepared to library using SureSelectXT Low Input Target Enrichment and Library Preparation system (#G9703-90000 Agilent USA) and sequenced on an Illumina NovaSeq-6000 sequencer (Illumina, San Diego, California, USA) to generate 150×150bp paired end reads. Image analysis and base calling was done using onboard RT3 software (Illumina, San Diego, California, USA). Somatic single-nucleotide variants, Indel and copy number variation (CNV) were determined using the MuTect/ANNOVAR/dbNSFP31, VarscanIndel and CNVnator software. TMB calculation was based on the protocol of Foundational Medicine.<sup>17</sup> Based on its detection protocol of Bayesian methodology, reads with variant allele frequency (VAF)≥5% were preserved. Mutations with VAF greater than 5% made major contribution to TMB, and mutations with VAF <5% were caused by artefacts and usually filtered out before neoantigen prediction according to a FDA summary (PMA: P170019).

Data of WES-sequence above were obtained and sent to Qianyang Biomedical Research Institute, Shenzhen, China for neoantigen sequencing and predicted peptides bioinformatics analysis. All patients' Phased Somatic VCF files were analysed by software pVACseq limited to MHC-I alleles (HLA-A, HLA-B and HLA-C alleles).<sup>18</sup> Epitopes were predicted based on variants from each patient, respectively. In brief, HLA typing was performed using OptiType (V.1.3.3). Based on the HLA alleles, pVACseq module in pVACtools (V.1.0.0) were used to predict the peptides binding to these alleles by using different prediction algorithms (NetMHCpan, NetMHC, NetMHCcons, PickPocket, SMM, SMMPMBEC, MHCflurry and MHCnuggets).<sup>18</sup> To get more specific peptides, median score of the eight algorithm results were calculated and regarded as MHC-I binding affinity, which was quantified as IC50 (nM); then epitopes with IC50 <50nM were retained.<sup>19-21</sup> Peptides with IC50 <50nM are considered as HANs. Customised peptides were obtained from Sangon Biotech (Shanghai, China).

### Survival data and analysis

For the OS analysis, the survival time was calculated from the time of pathogenesis until last contact or death. The censoring proportion of survival data was 21 of 56 patients. We compared OS between low group and high group using the median frequency of all the indicators as a cut point. This cut point could fairly compare all the indicators in discriminating patient survival. For progression-free survival (PFS) analysis to assess the clinical efficiency of anti-PD-1 treatment, the evaluation criterion referred to imRECIST Refining Guidelines<sup>22</sup> and the baseline of tumour size was set before the first time of immunotherapy. P values were determined using log-rank test.

### Flow cytometry for TILs

Tumour samples were cut into small pieces and digested in RPMI-1640 supplemented with collagenase at 1mg/mL (#C1889 Sigma USA). Digestion lasted for 1 hour at room temperature and filtered through a 70 µm filter. Single-cell suspensions were surface stained in fluorescence activated cell sorter (FACS) buffer (phosphate buffer solution (PBS), supplemented with 1% fetal bovine serum (FBS)) with the following antibodies for flow cytometric analysis, including FITC Zombie Green (#423 111 Biolegend USA), PE Anti-human CD3 (#344 806 Biolegend USA), APC Anti-human CD8 (#344 721 Biolegend USA), Brilliant Violet 421 Anti-human CD39 (#328 214 Biolegend USA),

PE-Cy7 Anti-human PD-1 (#561 272 BD USA). Flow data were analysed by FlowJo V.10.0.

### TIL ex vivo expansion and autologous tumour organoid culture

Samples of needle biopsy from patients with HCC were segregated into average two parts. One part was used for TIL expansion. TILs were generated and cultured as previously described.<sup>23</sup> Briefly, tumour samples were cut into small pieces in X-Vivo 15 Lymphocyte medium (#04-418Q Lonza Switzerland). IL-2 (#200-02-50 PerproTech USA) at 6000 IU/mL was used for TIL expansion. All cells were cultured at 37°C with 5% CO<sub>2</sub> for 2 weeks. After expansion, TILs were collected and sorted as the marker CD39 and CD8 by FACS for the following experiments. Another part of tumour sample was used for organoid culture. HCC organoids were established as the protocol previously described.<sup>24</sup> Organoids were passaged approximately every week (not exceed five generations before using). All organoids were regularly checked for mycoplasma contamination using the MycoAlert Mycoplasma Detection Kit (#CUL001B R&D USA).

### Preparation of peptide-pulsed antigen-presenting cells (APCs)

Autologous CD14<sup>+</sup> DCs were sorted from peripheral blood mononuclear cell (PBMCs) by EasySep Human CD14 Pos Selection Kit (#17 858 Stemcell USA) and incubated with DC medium (RPMI 1640 medium supplemented with 10% FBS, 2 mM L-glutamine, 800 IU/mL GM-CSF (#300-03-100 Peprotech USA) and 200 U/mL IL-4 (#200-04-50 Peprotech USA). All peptides were synthesised to pulse APCs individually. Autologous DCs were harvested, washed and resuspended at 1.0 × 10<sup>6</sup> cells/mL in DC medium and incubated with 10 µg/mL of the individual peptide for overnight at 37°C at 5% CO<sub>2</sub>. Following pulsing, the APCs were centrifuged, resuspended in fresh DC medium without cytokines in concentration 2 × 10<sup>6</sup> cells/mL and used for coculture assays.

### TILs and APCs coculture assay and IFN-γ ELISPOT assay

Expanded TILs were incubated with peptide-pulsed APCs at a ratio of 1:2. In addition, no peptide dimethyl sulphoxide (DMSO) pulsed APCs were used as negative control, with OKT3 (#05121-25-500 Peprotech USA) (10 µg/mL) was used as positive control. Before coculture, the IL-2 containing medium for TILs expansion was removed, and the TILs were resuspended in IL-2 free medium to rest for 24 hours. Then 100 µL of TILs and APCs were mixed together for total volume of 200 µL/well IL-2 free medium in 96-well interferon-γ (IFN-γ) ELISPOT plates (#3420-2 hour Mabtech Sweden) for 24 hours. Each ELISPOT plate was scanned and counted using an ImmunoSpot plate reader and associated software (Cellular Technologies).

### Organoid killing assay

Organoids were harvested and part of the organoids were dissociated into single cells and counted to infer the number of tumour cells to allow a effector:target (E:T)=10:1 ratio. Tumour organoids were resuspended in IL-2 free human HCC organoids medium and seeded in flat-bottom plate with 1 × 10<sup>5</sup> autologous CD39<sup>+</sup>/CD8<sup>+</sup>TILs obtained by sorting. To facilitate visualisation, organoids were previously stained with 1 mM of Cell-Trace Farred (#C34572 Invitrogen USA). At the start of coculture, caspase 3/7 probe (#C10723 Invitrogen USA) was added at 1:2000 dilution to visualise cell apoptosis. After 24 hours of coculture, microphotographs images were taken. The supernatant and cells were collected for following test. Organoids were

dissociated into single cells and washed in FACS buffer and stained with PE anti-human CD137 (#309 803 Biolegend USA) and Pacific Blue anti-human CD107a (#328 623 Biolegend USA) for 30 min. Cells were washed twice prior to flow cytometric recording. Supernatant was used to examine the IFN-γ secretion by ELISA (#430 107 Biolegend USA).

### Peptide stimulation and antigen-specific T cells culture

Based on the above analysis, 6 patients were selected from the 12 candidate patients. Further selected mutant type (MT)/wild type (WT) peptides are listed in table 1 and synthesised. Patients' autologous PBMCs were used to evaluate the immunogenicity of candidate peptides in vitro. An established culture protocol was mainly used in detecting peptide-specific cytotoxic T lymphocyte (CTLs) as previously reported.<sup>25 26</sup> Briefly, blood samples were obtained from patients for the isolation of PBMC by centrifugation and suspended in X-Vivo15 medium. In each well 1 × 10<sup>5</sup> PBMCs was incubated with a corresponding peptide (25 µM) in 200 µL culture medium with IL-2 (150 U/mL) in U-bottomed wells. At 3-day intervals, half of the culture medium containing peptide (25 µM) and IL-2 (150 U/mL) was changed. On day 10, the specific T cell responses to each peptide were collected. CD8<sup>+</sup> T cells were sorted by EasySep Human CD8<sup>+</sup> T Cell Isolation Kit (#17985 Stemcell USA). Cells were washed twice and then cocultured with autologous tumour organoid for 24 hours. Before coculture, organoids were stained with 1 mM of Cell-Trace Farred. At the start of coculture, caspase 3/7 probe was added at 1:2000 dilution. Organoids were seeded in flat-bottom plate with 1 × 10<sup>5</sup> CD8<sup>+</sup> T cells. T cells and organoids were at a E:T=10:1 ratio. No peptide was regarded as negative control. Twenty-four hours later, microphotograph images were taken and supernatant was collected to examine the IFN-γ secretion by ELISA. In addition, organoids were dissociated into single cell. Cells were washed in FACS buffer and stained with PE anti-human CD8 (#344 743 Biolegend USA), PerCP/Cy5.5 anti-human CD39 (#328 217 Biolegend USA) and Brilliant Violet 421 anti-human CD137 (#309 819 Biolegend USA) for 30 min. Cells were washed twice prior to flow cytometric recording.

### Statistical analysis

Pearson's correlation coefficient was used to evaluate the correlation matrices. Survival curves were generated using Kaplan-Meier estimates and tested using the log-rank test. Data samples were compared using a two-tailed Student's t test, and a p value of less than 0.05 was considered significant.

## RESULTS

### The value of HAN is correlated with better OS in patients with HCC

First, the clinical data and gene mutations of 56 patients with HCC were obtained by WES analysis (figure 1A). The top 20 high-frequency mutant genes were identified, including TP53 (50%), CTNBN1 (18%), ARID1A (16%) and AXIN1 (11%). HANs were defined as neoantigens with high MHC-I peptide-binding affinity and mutant type IC<sub>50</sub> < 50 nM (figure 1B). Then, patients were segregated into high and low groups stratified above or below the median of the indicators above. Our results showed that the value of HAN were significantly correlated with OS (*p*=0.0199), but TMB (*p*=0.7505) or neoantigen (*p*=0.2297) did not (figure 1C–E). The 5-year survival rate of patients with HAN-high group (60.76%, *p*=0.0199) was better than patients with HAN-low group (38.76%, *p*=0.0199) (figure 1E). These results suggest HAN can be used as a prognostic biomarker for patients with HCC.



**Table 1** Candidate top five peptides according to the binding-affinity of HLA-I alleles (MT IC50 and WT IC50) from three patients in HAN-high group and HAN-low group

	Gene	CDNA change	AA change	HLA allele	MT peptide	MT IC50	WT peptide	WT IC50
HCC14	VCX	595G>C	Glu199Gln	HLA-A*02:06	SQMEELPSV	1.7	SEMEELPSV	23.3
	CHST3	832C>T	Arg278Trp	HLA-A*02:06	WQLEFLQPL	2.3	RQLEFLQPL	3.4
	OR10G8	53C>T	Ala18Val	HLA-A*02:06	FILMGLPHV	2.4	FILMGLPHA	6
	DYNC1H1	7828C>T	Arg2610Trp	HLA-A*02:06	TLFSALWAL	3.8	TLFSALRAL	129.2
	CYB561D1	209A>T	Glu70Val	HLA-A*02:06	WVMPVIPAL	4.1	WVMPPEIPAL	4.5
HCC31	TAS2R30	935G>G	Thr312Arg	HLA-A*31:01	RSLRLHRFR	4.2	RSLRLHRFT	4837.8
	TRIM68	1201G>A	Gly401Arg	HLA-A*31:01	RLRKRNEYR	5.3	RLRKGNEYR	6.8
	SLC4A4	1588G>A	Gly530Arg	HLA-A*31:01	STRPVLVFER	5.6	STGPVLVFER	93.1
	ABCA2	1640C>T	Ser547Leu	HLA-C*03:04	FLPSGMAL	5.8	FSLPSGMAL	2.3
	GUCY1A3	619C>T	Pro207Ser	HLA-A*31:01	HVYFFSKR	7	HVYFFPKR	11.2
HCC04	SLC26A11	664G>A	Val222Met	HLA-A*02:03	LMRDHMPV	3.3	LMRDHVPPV	23.3
	TAS1R1	782G>A	Arg261His	HLA-A*02:03	CLMHHLAQA	3.4	CLMRHLAQA	4
	OR7G1	467C>T	Ala156Val	HLA-A*02:03	FMSTMDVLV	4.1	FMSTMDALV	3.2
	ADCY1	1975C>T	Arg659Trp	HLA-A*02:03	VLYLHITWV	4.9	VLYLHITRV	4.4
	OR10G8	53C>T	Ala18Val	HLA-A*02:03	FILMGLPHV	5.1	FILMGLPHA	200
HCC18	XKR4	122G>T	Gly41Val	HLA-A*02:01	GLAPGLPSV	3.4	GLAPGLPSG	2422.8
	TAS2R46	893G>C	Arg298Thr	HLA-A*02:01	VLWHVYVW	5.5	VLWHVRYVW	15
	CSNK1A1	929G>A	Arg310His	HLA-A*02:01	YMYLRQLFHI	8.2	YMYLRQLFRI	18
	ANKRD36C	1205T>C	Ile402Thr	HLA-A*11:02	IISKLYIPK	9.7	IISKLYIPK	15.7
	SYNPO	2769G>T	Lys923Asn	HLA-A*11:02	QVWNPSCFK	10.3	QVWKPSCFK	15.2
HCC28	FOXB1	712T>C	Tyr238His	HLA-B*35:01	MASGDHSAY	2.6	MASGDYSAY	2.4
	MIF4GD	185G>A	Arg62His	HLA-B*35:01	MPSHCNTQY	4.2	MPSRCNTQY	5.1
	AP2A1	445G>T	Ala149Ser	HLA-C*03:03	FASDIPRIL	5.4	FAADIPRIL	3.9
	SLC25A5	679A>G	Thr227Ala	HLA-B*35:01	TAVAGLASV	6	TAVAGLSV	8.2
	FRMD8	152C>G	Ser51Trp	HLA-B*35:01	LPWLSAHEL	12.9	LPLSAHEL	26.4
HCC21	NCOA3	600G>T	Leu200Phe	HLA-A*11:01	HTFNCRMEMK	4.5	HTFNCRMLMK	6.5
	HEATR3	740T>G	Leu247Arg	HLA-A*11:01	SSMESRLK	5.1	SSMESLLK	3.7
	NPIP815	1256T>C	Ile419Thr	HLA-A*11:01	ATRINPWVEK	10.4	AIRINPWVEK	22.6
	NBAS	4429G>C	Glu1477Gln	HLA-A*24:02	FYQSVISNPF	15.5	FYQSVISNPF	44.8
	RAG1	15C>A	Phe5Leu	HLA-C*12:02	MAASLPPTL	28	MAASFPTL	20.8

HAN, high-affinity neoantigen; HCC, hepatocellular carcinoma.

### The value of HAN is positively correlated with the frequency of CD39<sup>+</sup>CD8<sup>+</sup> TILs

Recent studies have shown that the frequency of CD39<sup>+</sup>CD8<sup>+</sup> TILs has a positive correlation with OS in head and neck squamous cell carcinoma.<sup>14</sup> To explore whether HANs were associated with CD39, the frequency of CD39<sup>+</sup>CD8<sup>+</sup> TILs was investigated by flow cytometry (figure 2A–C). Significantly, the value of HAN was better correlated with the frequency of CD39<sup>+</sup>CD8<sup>+</sup> TILs ( $R^2=0.6786$ ) than TMB ( $R^2=0.3072$ ) or neoantigen ( $R^2=0.5515$ ) (figure 2D–F). Furthermore, a higher frequency of CD39<sup>+</sup>CD8<sup>+</sup> TILs was positively correlated with better OS (5 year survival: 56.51% vs 46.42%;  $p=0.0365$ ) (figure 2G). In conclusion, our findings indicated that the value of HAN is positively correlated with the frequency of CD39<sup>+</sup>CD8<sup>+</sup> TILs.

### CD39<sup>+</sup>CD8<sup>+</sup> TILs from HAN-high group show better antitumour activity

To investigate whether CD39<sup>+</sup>CD8<sup>+</sup> TILs have the capability of tumour-killing, CD39<sup>+</sup>CD8<sup>+</sup> TILs were sorted after expansion in vitro and then cocultured with autologous tumours organoids for 24 hours to assess killing efficiency, respectively (figure 3A). All the cases were divided into HAN-high and low groups according to the median of HAN value. Six candidate patients were selected from each group for further study (online

supplemental figure 1). Details of high-affinity peptides and HLA alleles of candidate patients are shown (table 1 and online supplemental figure 2).

The results showed that CD39<sup>+</sup>CD8<sup>+</sup> TILs from HAN-high group induced more caspase3/7 positive apoptosis than those from the HAN-low group ( $36.03\% \pm 6.029\%$  vs  $14.15 \pm 3.294\%$ ,  $p=0.0003$ ) in HCC organoids (figure 3B–D), whereas CD39<sup>-</sup>CD8<sup>+</sup> TILs of either group induced little apoptosis (figure 3B–D). Furthermore, the frequency of T cell effector markers CD107a and CD137 was higher in CD39<sup>+</sup>CD8<sup>+</sup> TILs from the HAN-high group than those from the HAN-low group (CD107a:  $33.13 \pm 6.535\%$  vs  $13.04 \pm 2.893\%$ ,  $p=0.0184$ ; CD137:  $28.20 \pm 4.016\%$  vs  $11.60 \pm 2.667\%$ ,  $p=0.0063$ ) (figure 3E–G). These findings suggest that CD39<sup>+</sup>CD8<sup>+</sup> TILs from HAN-high group had better antitumour ability compared with those from HAN-low group.

To further confirm aforesaid findings in fresh CD39<sup>+</sup>CD8<sup>+</sup> TILs, surgically removed HCC fresh tumour samples from patients (online supplemental table 2) were prepared for cell suspension and detected by flow cytometry immediately. Our data confirmed that CD39<sup>+</sup>CD8<sup>+</sup> TILs from fresh tumour in HAN-high group showed a better antitumour activity than those in HAN-low group (online supplemental figure 3A–H), which was consistent with the findings of expanded TILs. Furthermore, the expansion before or after sorting for TILs had no bias in





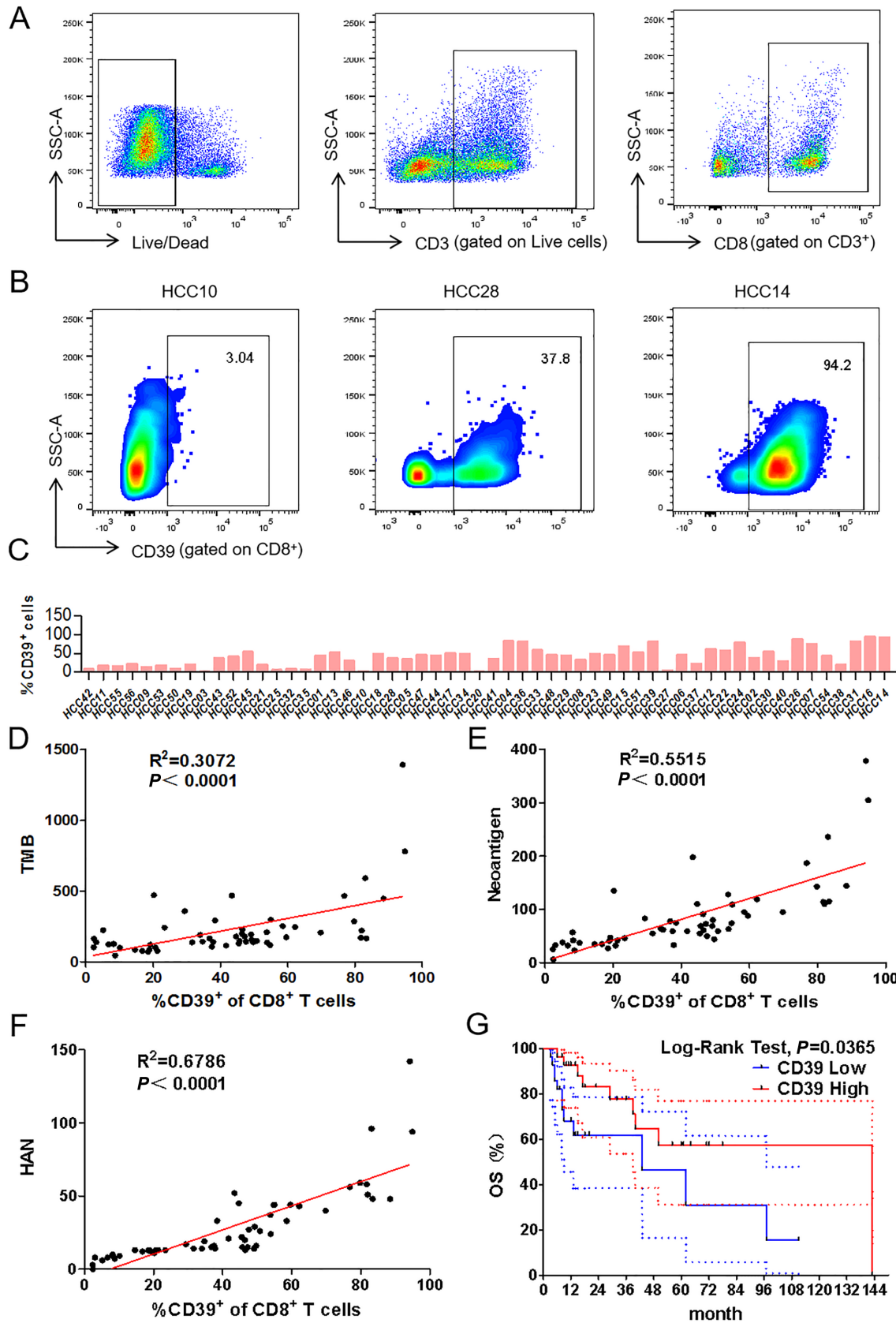


**Figure 2** Correlation analysis between frequency of CD39<sup>+</sup>CD8<sup>+</sup> TILs and value of TMB, neoantigen or HAN. (A,B) Representative gating strategy for CD8<sup>+</sup> TILs of patients with HCC by flow cytometry. Numbers in gates indicate the percentage of CD39<sup>+</sup>CD8<sup>+</sup> TILs. (C) Frequency of CD39<sup>+</sup>CD8<sup>+</sup> TILs of each patient was detected by flow cytometry. (D–F) Correlation between frequency of CD39<sup>+</sup>CD8<sup>+</sup> TILs and TMB, neoantigen or HAN estimated by liner regression. (G) Patients were segregated into CD39<sup>+</sup> high and low group based on above or below the median frequency (43.4%) of CD39 expression. The survival curves were analysed by log-rank test ( $p < 0.05$  was considered significant). The dotted-line indicated the 95% CI. HAN, high-affinity neoantigen; HCC, hepatocellular carcinoma; TMB, tumour mutational burden.

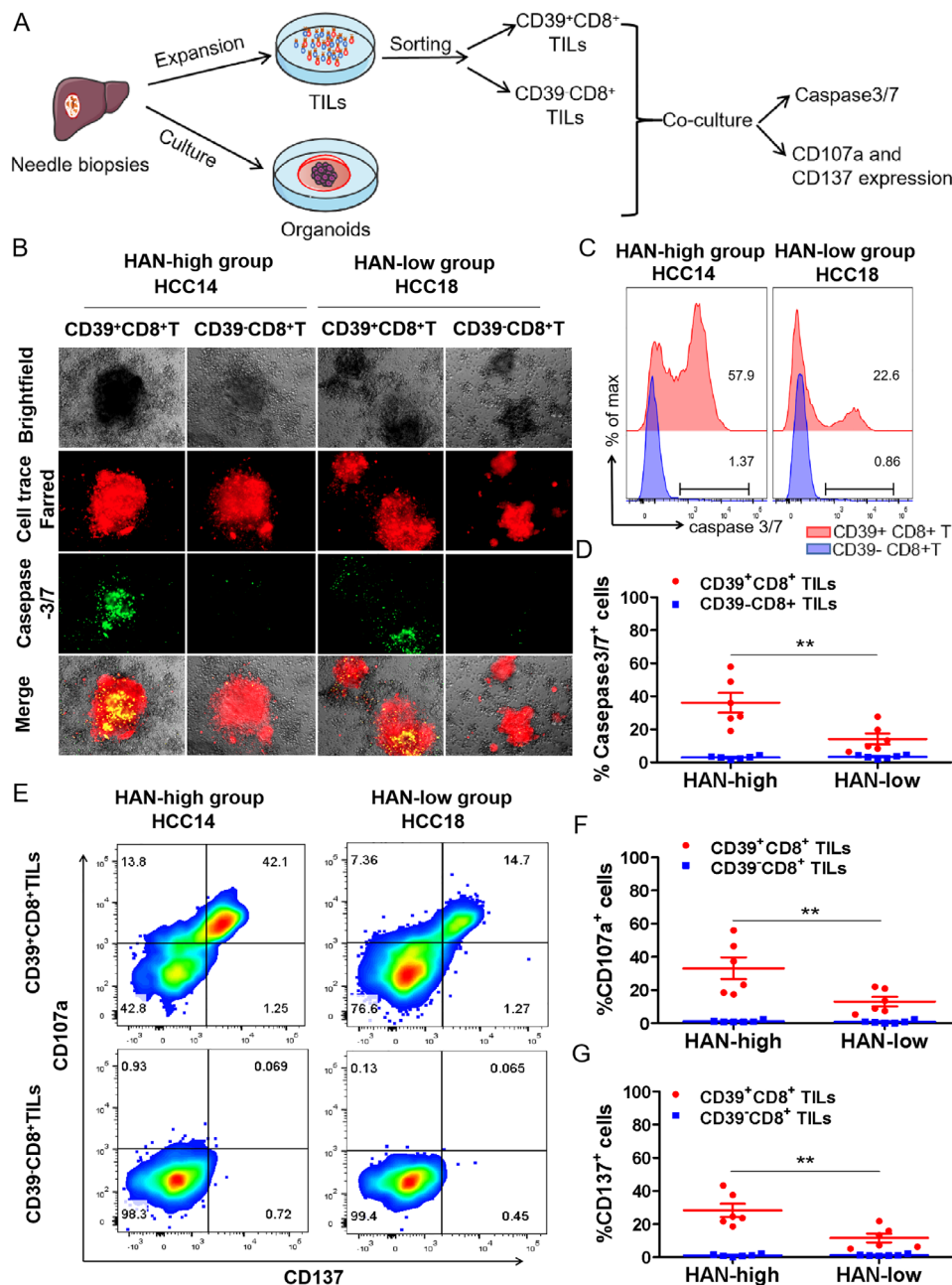


**Figure 3** CD39<sup>+</sup>CD8<sup>+</sup> TILs from HAN-high group showed stronger antitumour activity. (A,B) CD39<sup>+</sup>CD8<sup>+</sup> TILs of candidate patients from HAN-high/low groups were expanded and sorted *in vitro* and then cocultured with autologous tumours organoids for 24 hours to assess killing efficiency respectively. Organoids (red) were labelled with Cell-Trace FarRed, and apoptotic cells (green) were labelled with caspase-3/7 probe. Microphotograph images of one representative from each group are shown. Scale bars, 40  $\mu$ m. (C,D) Flow cytometry was to analyse killing efficiency by FITC signal (caspase 3/7 probe). Summary of the frequency of caspase3/7<sup>+</sup> for representative six patients from each group was shown. The dots represent different patients. (E,G) Flow cytometry plots was to analyse T cell effector marker CD107a and CD137 on CD39<sup>+</sup>CD8<sup>+</sup> T cells. Summary of the frequency of CD107a and CD137 positive was shown for representative patients from each group. The dots represent different patients. Data are presented as mean $\pm$ SEM (n=6), \*P<0.05, \*\*p<0.01. HAN, high-affinity neoantigen; HCC, hepatocellular carcinoma.

IFN- $\gamma$  production and CD137 and CD107a expression (online supplemental figure 4A,B).

#### HAN-specific T cells are identified in CD39<sup>+</sup>CD8<sup>+</sup> TILs

To explore whether tumour-reactive CD39<sup>+</sup>CD8<sup>+</sup> TILs were induced by the effective stimulation of HANs, CD39<sup>+</sup>CD8<sup>+</sup> TILs and CD39<sup>-</sup>CD8<sup>+</sup> TILs were sorted from two candidate patients for HAN-specific CD8<sup>+</sup> T cell identification assay, respectively, and cocultured with autologous DCs pulsed

by candidate peptides from patient HCC14 and HCC18, after which IFN- $\gamma$  production was tested by ELISPOT assay (figure 4A). Our results demonstrated that two peptides from patient HCC14 (TLSFALWAL, WVMPVIPAL) and one from patient HCC18 (YMYLRQLFHI) induced significant peptide-specific T-cell responses in CD39<sup>+</sup>CD8<sup>+</sup> TILs group, but no detectable responses were observed in CD39<sup>-</sup>CD8<sup>+</sup> TILs group, which suggest that peptide-specific T-cell were identified in CD39<sup>+</sup>CD8<sup>+</sup> TILs group (figure 4B–D). Besides, all the WT



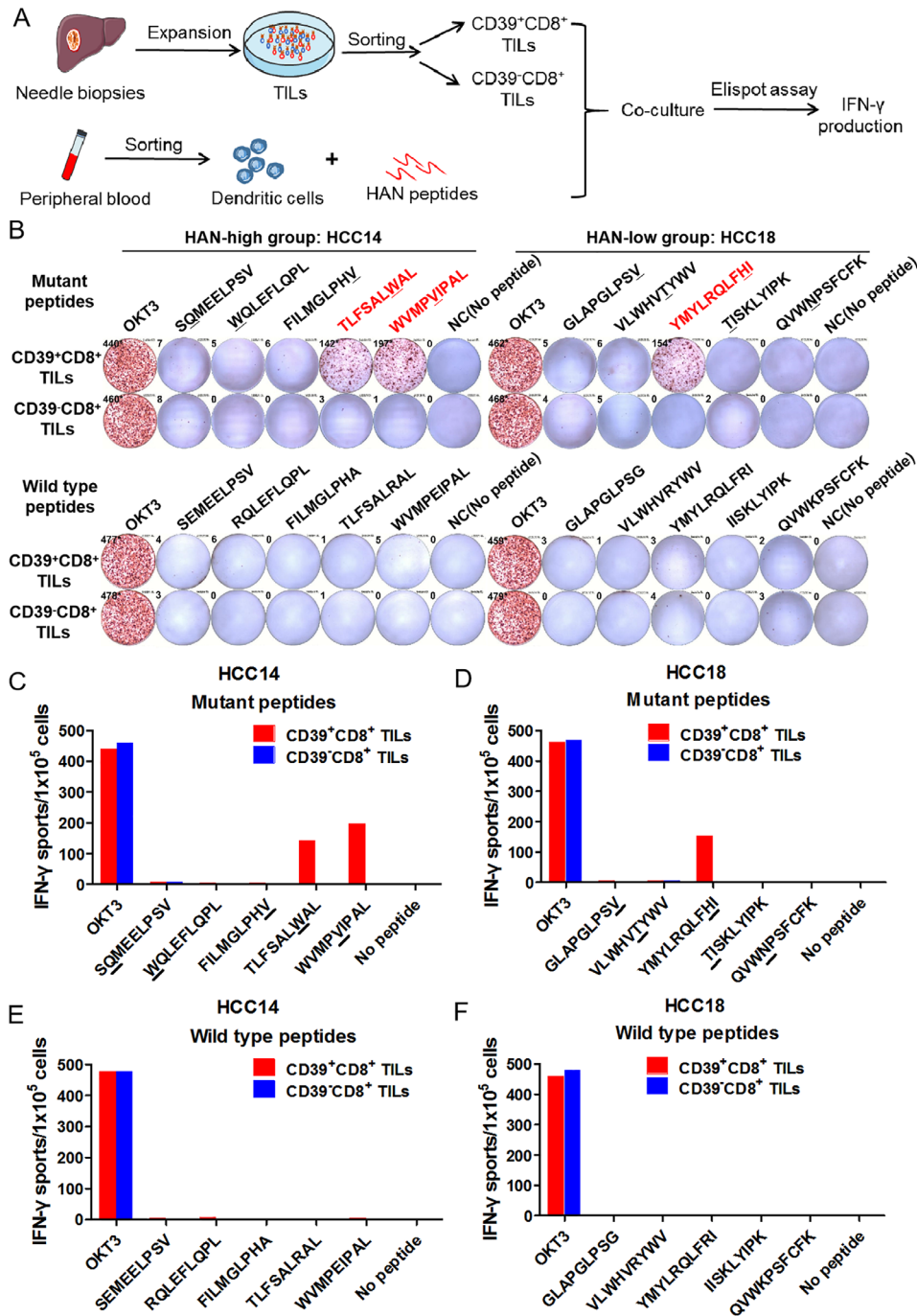


**Figure 4** Neoantigen-specific T cells were identified in CD39<sup>+</sup>CD8<sup>+</sup> TILs. (A,B) CD39<sup>+</sup>CD8<sup>+</sup> TILs of candidate patients from HAN-high/low groups were expanded and sorted in vitro and then cocultured with autologous DC cells pulsed by top five HANs (mutant peptides) or corresponding wild type peptides from patient HCC14 and HCC18, and IFN-γ production was determined by ELISPOT assay. The mutated amino acids of each mutant peptide were indicated by the underline. (C–F) The number of IFN-γ spots/1×10<sup>5</sup> cells in each group. DC, dendritic cell; HAN, high-affinity neoantigen; HCC, hepatocellular carcinoma.

peptides failed to induce the IFN-γ secretion (figure 4E,F). In other words, HAN-specific CD8<sup>+</sup> T cells were enriched in CD39<sup>+</sup>CD8<sup>+</sup> TILs.

**HAN-peptides activate tumour-reactive CD39<sup>+</sup>CD8<sup>+</sup> T cells from PBMCs**

Based on aforementioned findings, we hypothesised that there would be more tumour-specific HANs in patients of HAN-high group that can generate CD39<sup>+</sup>CD8<sup>+</sup> T cells with better

tumour-reactive activity by PBMCs and peptide coculture. To verify this hypothesis, PBMCs from each patient were stimulated with the corresponding peptides in vitro and were sorted by CD8 magnetic beads on day 10. Subsequently, CD8<sup>+</sup> T cells were cocultured with autologous tumour organoids for 24 hours. Antitumour activity was assessed by measuring IFN-γ secretion (figure 5A). In HAN-high group, two peptides (TLFSALWAL, WVMPVIPAL) in patient HCC14, two (RLRKRNEYR, FLLPSGMAL) in HCC31 and one (LMRDHMPPV) in HCC04

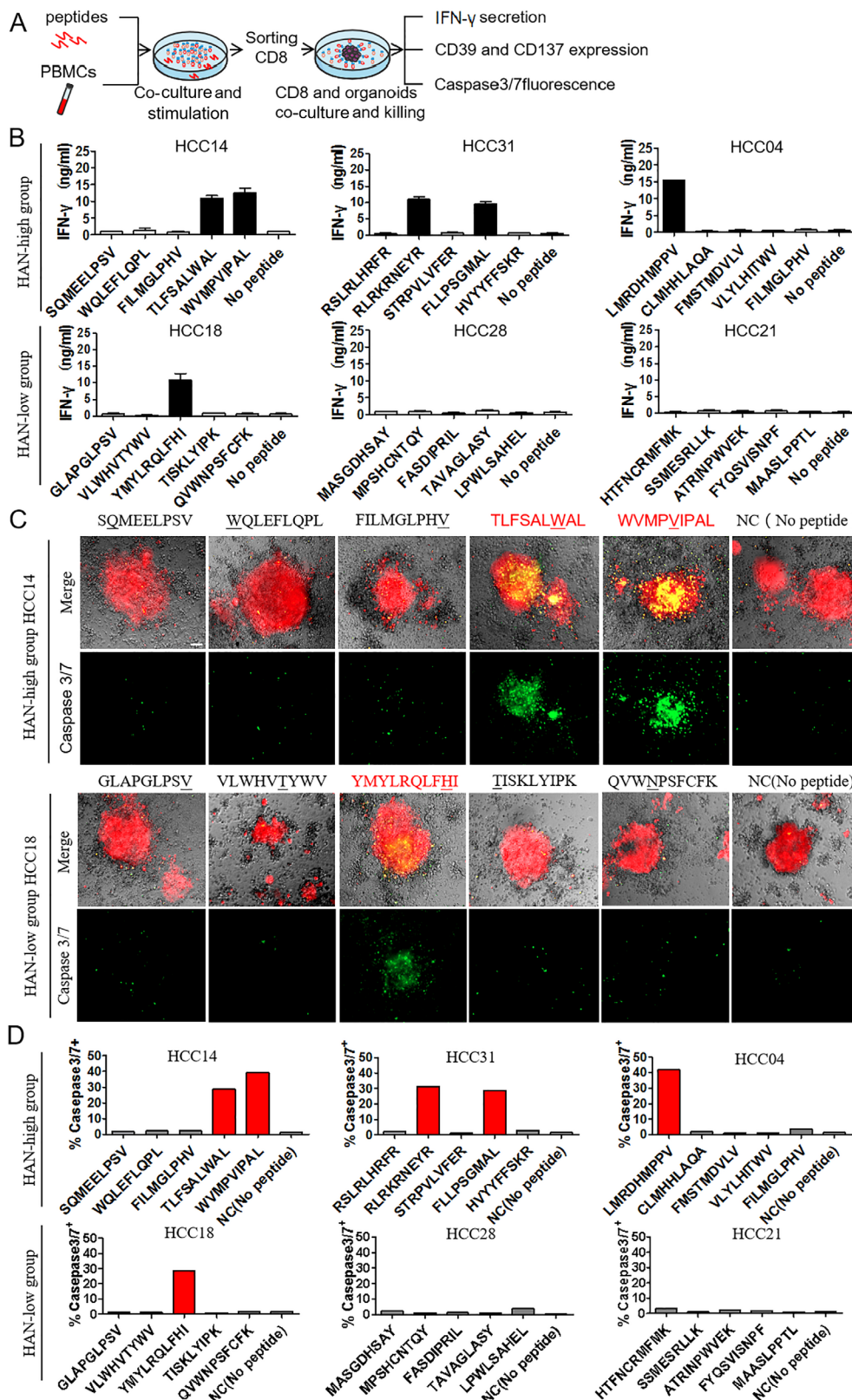


**Figure 5** Induction of tumour-reactive CD39<sup>+</sup>CD8<sup>+</sup> T cells by stimulation with candidate HANs from PBMCs. (A) Autologous PBMCs of candidate patients from HAN-high/low groups were stimulated by top five HANs, and on day 10 CD8<sup>+</sup> T cells were sorted and cocultured with autologous tumour organoids for 24 hours. (B) Tumour recognition was assessed by measuring IFN- $\gamma$  secretion of supernate. No peptide stimulation was tested as control. Data were presented as mean $\pm$ SEM (n=3). (C) CD8<sup>+</sup> T cells stimulated with HANs from HAN-high/low groups were cocultured with autologous organoids, which were labelled with Celltrace-Farred (red) prior to coculture. Tumour apoptosis was detected by green-fluorescent caspase-3/7 probe, thus apoptotic cells in organoids were indicated in yellow after merge. No peptide stimulation was tested as control. Microphotographs images were one representative patient for each two groups. (D) Summary of killing efficiency of caspase3/7 signal frequency for all the six representatives from each two groups. HAN, high-affinity neoantigen; HCC, hepatocellular carcinoma.

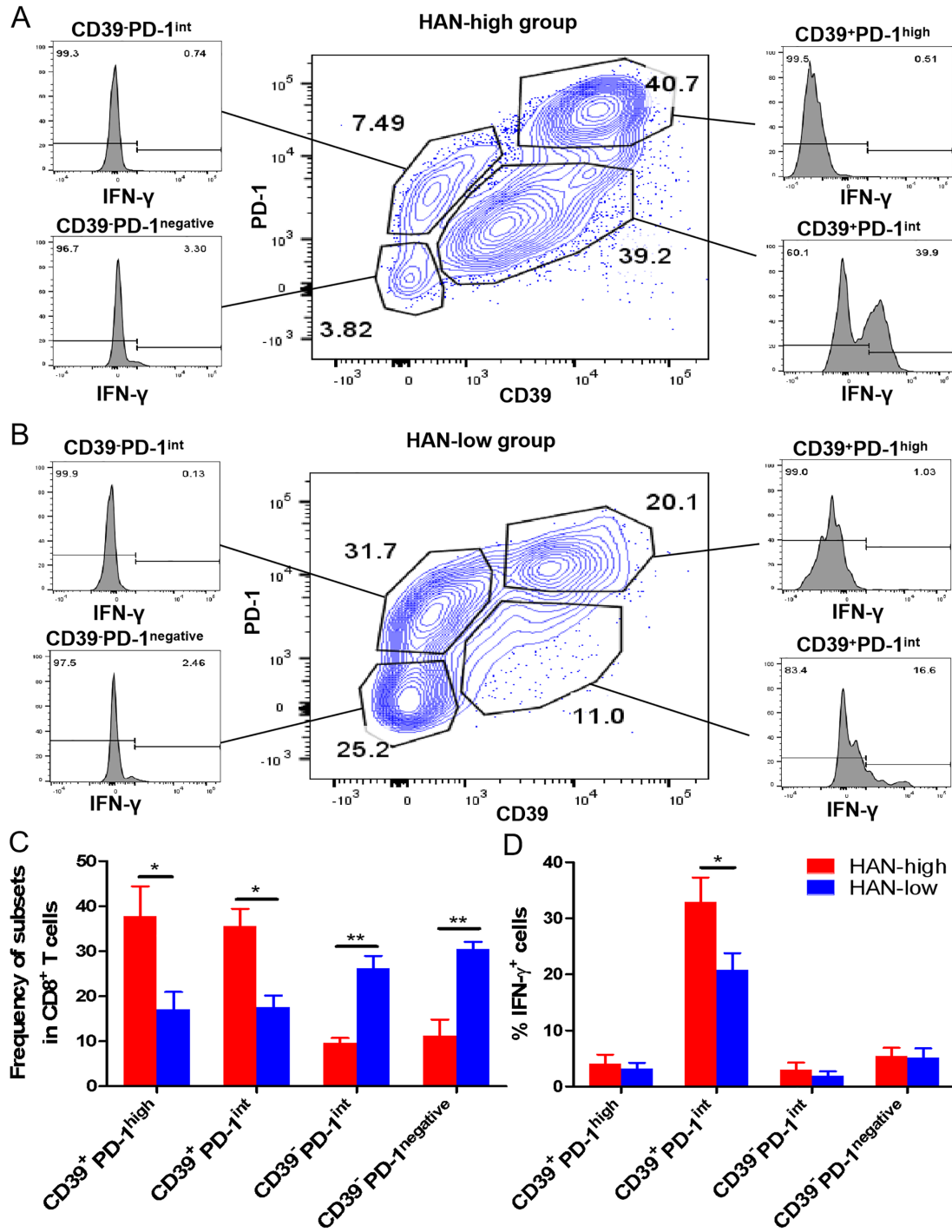


**Figure 6** The phenotype analysis of CD39<sup>+/-</sup>PD-1<sup>high/int/negative</sup>CD8<sup>+</sup> TILs. (A,B) Flow cytometry analysed the CD39<sup>+/-</sup>PD-1<sup>high/int/negative</sup> subsets gated from CD8<sup>+</sup> TILs in fresh HCC tissues from 12 patients. The frequency of IFN- $\gamma$ <sup>+</sup> from each subsets was revealed. (C,D) Statistic graphs of frequency of each subset and IFN- $\gamma$ <sup>+</sup> expression were shown. Red bars represented HAN-high group and blue bars represented HAN-low group. Data are presented as mean $\pm$ SEM (n=6), \*P<0.05, \*\*p<0.01. HAN, high-affinity neoantigen; HCC, hepatocellular carcinoma; PD, progress disease.

induced significant peptide-specific T-cell responses. Only one effective peptide (YMYLRQLFHI) in patient HCC18 from HAN-low group was identified to induce IFN- $\gamma$  secretion (figure 5B and online supplemental figure 5A,B). Furthermore, effective peptides from each group significantly increased CD39 and CD137 expression (online supplemental figure 6A,B), indicating that those effective peptides-induced antitumour response related to CD39<sup>+</sup>CD8<sup>+</sup> T cells activation. Moreover, autologous tumour organoids killing assay showed that those

effective peptides induced far more caspase3/7-mediated apoptosis in HCC organoids than the negative peptides did from either group (figure 5C,D), indicating a successful tumour-killing ability of CD8<sup>+</sup> T cells induced by those peptides, whereas allogeneic peptides could not induce IFN- $\gamma$  secretion for autologous tumour organoid killing, suggesting that peptide recognition is specific and its antitumour effects are personalised (online supplemental figure 7). In addition, RNA-seq data indicated that CD39<sup>+</sup>CD8<sup>+</sup> T cells exhibited effector T cell signatures after



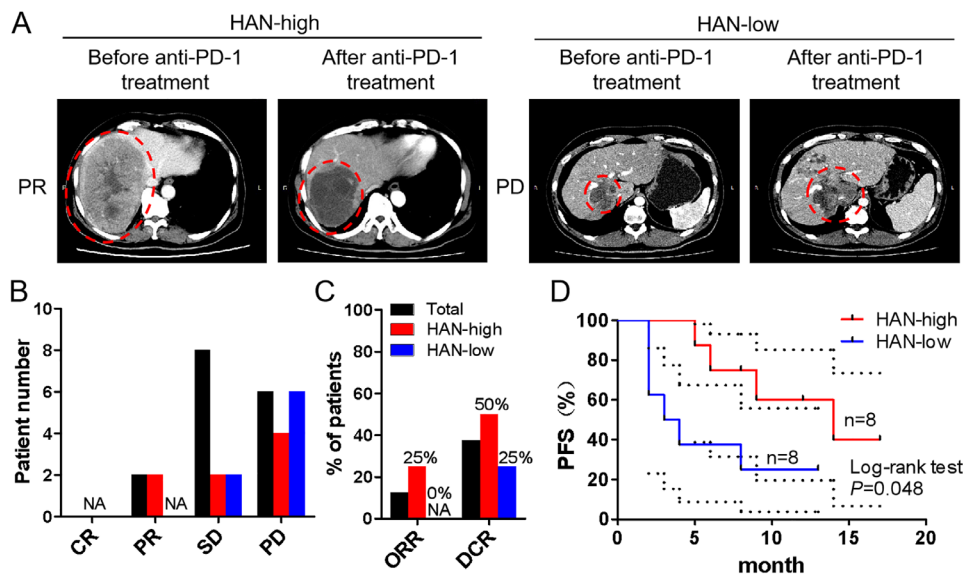


**Figure 7** Curative evaluation of HAN-high/low groups after anti-PD-1 therapy. Sixteen patients had taken anti-PD-1 therapy afterwards and were divided into HAN-high/low groups (8 vs 8). The baseline tumour size was set before the first time of immunotherapy. (A) CT scans of representative patients from two groups were performed before and after anti-PD-1 immunotherapy. The immunotherapy evaluation criteria referred to imRECIST Refining Guidelines. (B,C) The curative evaluation of immunotherapy of HAN-high/low groups was shown. (D) PFS of patients in HAN-high group compare to those in HAN-low group was shown. PFS curves were analysed by log-rank test ( $p=0.048$ ). The dotted-line indicated the 95% CI. CR, complete response; DCR, disease control rate; HAN, high-affinity neoantigen; ORR, objective response rate; PD, progress disease; PFS, progression-free survival; PR: partial response; SD: stable disease.

HAN peptide stimulation, with higher expression of cytotoxic, activation, chemotaxis and adhesion molecules (online supplemental figure 8).

Overall, our findings demonstrated that patients with HCC in the HAN-high group generated more tumour-specific peptides with high MHC-I binding affinity than those in the HAN-low group; they are likely responsible for the activation of tumour-reactive CD39<sup>+</sup>CD8<sup>+</sup> T cells.

#### CD39<sup>+</sup>PD-1<sup>int</sup>CD8<sup>+</sup> TILs show an effector T cell phenotype and stronger antitumour activity in HAN-high versus HAN-low group

It was still controversial whether CD39<sup>+</sup>CD8<sup>+</sup> T cells with high PD-1 expression exhibit effector or exhausted phenotype (online supplemental figure 8E). To confirm that, TILs from fresh tumours were analysed by flow cytometry. Data revealed that CD39<sup>+</sup>PD-1<sup>high</sup>CD8<sup>+</sup> TILs exhibited exhaustion phenotype for low IFN- $\gamma$  production, while CD39<sup>+</sup>PD-1<sup>int</sup> CD8<sup>+</sup> TILs exhibited effector phenotype for high IFN- $\gamma$  production (figure 6A–D). Furthermore, the number and antitumour activity of CD39<sup>+</sup>PD-1<sup>int</sup> subsets were upregulated in HAN-high versus HAN-low group (figure 6C).

#### HAN-high patients benefit more from anti-PD-1 treatment compared with HAN-low patients

According to aforesaid findings, we speculated that patients in HAN-high group who had a higher ratio of CD39<sup>+</sup>CD8<sup>+</sup> TILs may benefit more from anti-PD-1 treatment. To confirm this conjecture, eight patients from each group treated with anti-PD-1 antibody afterwards were included into study (online supplemental table 1). The baseline tumour size was set before the first time of immunotherapy, and the curative evaluation referred to imRECIST Refining Guidelines.<sup>22</sup> Data showed that objective regression rate (ORR) and disease control rate (DCR) were higher in HAN-high group than those in HAN-low group

(ORR: 25% vs 0%; DCR: 50% vs 25%) (figure 7A–C). Moreover, survival curves revealed that patients in HAN-high group had a better PFS than those in HAN-low group ( $p=0.048$ ) (figure 7D).

#### DISCUSSION

In the present study, the most striking discovery was that the value of HAN was correlated with a markedly better OS in patients with HCC, suggesting an important role for tumour antigen-specific CD8<sup>+</sup> TILs activation in limiting tumour growth in these patients. More importantly, more effective peptides were identified from HAN-high group, which played an important role in activating tumour-reactive CD39<sup>+</sup>CD8<sup>+</sup> T cell.

Recently, accumulating evidence has shown that neoantigens are responsible for tumour regression in patients receiving TIL therapy and in immune checkpoint inhibitor therapy in both mouse models and clinical settings.<sup>23–27</sup> However, the arithmetic used to filtrate dozens of efficient peptides from thousands of candidates needed to be improved. The pVACtools suite represents a novel arithmetic to calculate MHC-I-peptide binding affinity, which was used to evaluate efficient peptides. In our study, mutant types with IC<sub>50</sub> less than 50 nM were defined as HANs. The value of HAN showed strong correlation with better OS, whereas TMB and neoantigens showed no significant correlation with OS. Our findings were in accordance with previous studies showing that TMB was not correlated with predicted neoantigens in the HCC microenvironment and was not suitable as a predictive biomarker in HCC,<sup>428</sup> although higher TMB or neoantigens showed significant correlation with better OS in non-small-cell lung cancer (NSCLC) and melanoma.<sup>29–32</sup>

Recent studies identified CD39 as a novel biomarker to distinguish tumour-specific CD8<sup>+</sup> T cells,<sup>14</sup> which can recognise tumour neoantigen peptides, in contrast to bystander CD8<sup>+</sup> T cells.<sup>16</sup> In our study, CD39<sup>+</sup>CD8<sup>+</sup> TILs could recognise tumour-specific HANs, and higher frequency of CD39<sup>+</sup>CD8<sup>+</sup> TILs was

positively correlated with better OS. Similarly, the frequency of CD39 on CD8<sup>+</sup> T cells was also correlated with higher OS in other human solid tumours.<sup>14</sup>

Although some studies have identified CD39 as a marker for exhausted T cells because its downstream inhibitory marker CD73 generates adenosine,<sup>33,34</sup> some studies reported that CD39<sup>+</sup>CD8<sup>+</sup> TILs were not true sense of exhausted T cells for a particular profile of effector functions, higher IFN- $\gamma$  and CD137 production.<sup>14</sup> Though they coexpress high levels of inhibitory receptors (PD-1, Tim3, Lag3) and a lower proliferative capacity in microenvironment *in vivo*,<sup>35</sup> the effector function can be retrieved after expansion *in vitro*.<sup>14</sup> Our findings revealed that HANs triggered antitumour activity by activating tumour-reactive CD39<sup>+</sup>CD8<sup>+</sup> T cells. Patients from HAN-high group had higher ratios of tumour-reactive CD39<sup>+</sup>CD8<sup>+</sup> T cells, the expression of CD107a, CD137 and secretion of IFN- $\gamma$  were greatly increased in organoid coculture systems. More importantly, in tumour microenvironment of HCC, CD39<sup>+</sup>CD8<sup>+</sup> TILs could be divided into two distinct subsets: CD39<sup>+</sup>PD-1<sup>int</sup>CD8<sup>+</sup> TILs which displayed an effector phenotype, and CD39<sup>+</sup>PD-1<sup>high</sup>CD8<sup>+</sup> TILs which displayed an exhaustion phenotype. Our study first clarified the phenotype of distinct CD39<sup>+</sup>CD8<sup>+</sup> TIL subsets in the tumour microenvironment, which may correlate with the outcome of anti-PD-1 therapy.

HAN-high patients who had higher ratio of CD39<sup>+</sup>CD8<sup>+</sup> TILs may benefit more from those treated with anti-PD-1 antibody, which may retrieve antitumour function of CD39<sup>+</sup>CD8<sup>+</sup> TILs by blocking highly expressed PD-1 receptors.<sup>14,16,36</sup> In our study, the number and antitumour activity of CD39<sup>+</sup>PD-1<sup>int</sup>CD8<sup>+</sup> TILs were upregulated in HAN-high versus HAN-low group, which may explain the improved clinical outcomes of anti-PD-1 therapy in HAN-high versus HAN-low group. Our present findings tentatively confirmed the better prognosis of patients in HAN-high group after anti-PD-1 therapy, additional samples are still needed for verification in our future study. Moreover, those patients in HAN-high group may benefit from treatment with peptide vaccine immunotherapy by generating tumour-reactive CD39<sup>+</sup>CD8<sup>+</sup> T cells from PBMCs.

Neoantigen-based immunotherapy was frequently restricted to the inefficient screening of effective neoantigen peptides. In our study, HANs activated CD39<sup>+</sup>CD8<sup>+</sup> T cells more efficiently than neoantigens, for it was a furtherly filtrated from neoantigen. Previous studies reported that only 0.6%–2.0% of neoantigen peptides could be identified by autologous T cells from a pool of hundreds of peptides.<sup>8,37,38</sup> However, when the preliminary screening for HANs was applied, the screening efficiency increased significantly to 20%, allowing 2–3 out of 10 peptides to be identified.<sup>10</sup> Our data showed that more effective peptides were identified in HAN-high group than HAN-low group (5 vs 1), which could activate tumour-reactive CD39<sup>+</sup>CD8<sup>+</sup> T cells and induced tumour-killing activity.

In conclusion, this study demonstrated a novel assessment system for predicting prognosis based on HANs and the frequency of CD39<sup>+</sup>CD8<sup>+</sup> T cells, which could be used to develop selective HAN-based personalised antitumour therapy for HCC and screen the suitable patients for anti-PD-1 therapy.

**Acknowledgements** The authors thank Yajing Wang of the GenomiCare Biotechnology (Co. Ltd., Shanghai, 201210, China) for WES analysis and Zhihui Xi of Qianyang Biomedical Research Institute (Shenzhen, China) for assistance in bioinformatics sequencing and pVACTools analysis.

**Contributors** TL, JT and MW wrote the manuscript. TL, JT and JL designed experiments. TL and JT performed experiments, TL, JT, MW, WF, PZ, HZ and LS

analysed and interpreted the data. BZ, JW, JG and SW collected clinical samples and data. JL supervised the project.

**Funding** This work was supported by grants from National Natural Science Foundation of China (No. 81671797, No. 81971719), the major scientific and technological project of Guangdong Province (No. 2017B030308006), the major programme for tackling key problems of Guangzhou city (No. 201704020144).

**Competing interests** None declared.

**Patient consent for publication** Not required.

**Provenance and peer review** Not commissioned; externally peer reviewed.

**Data availability statement** Data are available on reasonable request. All data relevant to the study are included in the article or uploaded as supplementary information. The data used to support the findings of this study are included within the article.

**Supplemental material** This content has been supplied by the author(s). It has not been vetted by BMJ Publishing Group Limited (BMJ) and may not have been peer-reviewed. Any opinions or recommendations discussed are solely those of the author(s) and are not endorsed by BMJ. BMJ disclaims all liability and responsibility arising from any reliance placed on the content. Where the content includes any translated material, BMJ does not warrant the accuracy and reliability of the translations (including but not limited to local regulations, clinical guidelines, terminology, drug names and drug dosages), and is not responsible for any error and/or omissions arising from translation and adaptation or otherwise.

**Open access** This is an open access article distributed in accordance with the Creative Commons Attribution Non Commercial (CC BY-NC 4.0) license, which permits others to distribute, remix, adapt, build upon this work non-commercially, and license their derivative works on different terms, provided the original work is properly cited, appropriate credit is given, any changes made indicated, and the use is non-commercial. See: <http://creativecommons.org/licenses/by-nc/4.0/>.

#### ORCID iD

Jiaping Li <http://orcid.org/0000-0003-2927-8877>

#### REFERENCES

- Villanueva A. Hepatocellular carcinoma. *N Engl J Med* 2019;380:1450–62.
- Jones NL, Xiu J, Rocconi RP, et al. Immune checkpoint expression, microsatellite instability, and mutational burden: identifying immune biomarker phenotypes in uterine cancer. *Gynecol Oncol* 2020;156:393–9.
- Hellmann MD, Ciuleanu T-E, Pluzanski A, et al. Nivolumab plus ipilimumab in lung cancer with a high tumor mutational burden. *N Engl J Med* 2018;378:2093–104.
- Dhanasekaran R, Nault J-C, Roberts LR, et al. Genomic medicine and implications for hepatocellular carcinoma prevention and therapy. *Gastroenterology* 2019;156:492–509.
- Zhu AX, Finn RS, Edeline J, et al. Pembrolizumab in patients with advanced hepatocellular carcinoma previously treated with sorafenib (KEYNOTE-224): a non-randomised, open-label phase 2 trial. *Lancet Oncol* 2018;19:940–52.
- Cheng A-L, Hsu C, Chan SL, et al. Challenges of combination therapy with immune checkpoint inhibitors for hepatocellular carcinoma. *J Hepatol* 2020;72:307–19.
- Gubin MM, Zhang X, Schuster H, et al. Checkpoint blockade cancer immunotherapy targets tumour-specific mutant antigens. *Nature* 2014;515:577–81.
- Robbins PF, Lu Y-C, El-Gamil M, et al. Mining exomic sequencing data to identify mutated antigens recognized by adoptively transferred tumor-reactive T cells. *Nat Med* 2013;19:747–52.
- Tran E, Ahmadzadeh M, Lu Y-C, et al. Immunogenicity of somatic mutations in human gastrointestinal cancers. *Science* 2015;350:1387–90.
- Chen F, Zou Z, Du J, et al. Neoantigen identification strategies enable personalized immunotherapy in refractory solid tumors. *J Clin Invest* 2019;129:2056–70.
- Tran E, Robbins PF, Lu Y-C, et al. T-Cell transfer therapy targeting mutant KRAS in cancer. *N Engl J Med* 2016;375:2255–62.
- Stevanović S, Pasetto A, Helman SR, et al. Landscape of immunogenic tumor antigens in successful immunotherapy of virally induced epithelial cancer. *Science* 2017;356:200–5.
- Yang R, Cheng S, Luo N, et al. Distinct epigenetic features of tumor-reactive CD8<sup>+</sup> T cells in colorectal cancer patients revealed by genome-wide DNA methylation analysis. *Genome Biol* 2019;21:2.
- Duhen T, Duhen R, Montler R, et al. Co-expression of CD39 and CD103 identifies tumor-reactive CD8 T cells in human solid tumors. *Nat Commun* 2018;9:2724.
- Lin R, Zhang H, Yuan Y, et al. Fatty Acid Oxidation Controls CD8<sup>+</sup> Tissue-Resident Memory T-cell Survival in Gastric Adenocarcinoma. *Cancer Immunol Res* 2020;8:479–92.
- Simoni Y, Becht E, Fehlings M, et al. Bystander CD8<sup>+</sup> T cells are abundant and phenotypically distinct in human tumour infiltrates. *Nature* 2018;557:575–9.
- Meléndez B, Van Campenhout C, Rorive S, et al. Methods of measurement for tumor mutational burden in tumor tissue. *Transl Lung Cancer Res* 2018;7:661–7.

- 18 Hundal J, Kiwala S, McMichael J, *et al.* pVACtools: a computational toolkit to identify and visualize cancer neoantigens. *Cancer Immunol Res* 2020;8:409–20.
- 19 Hundal J, Kiwala S, Feng Y-Y, *et al.* Accounting for proximal variants improves neoantigen prediction. *Nat Genet* 2019;51:175–9.
- 20 Hundal J, Carreno BM, Petti AA, *et al.* pVAC-Seq: a genome-guided in silico approach to identifying tumor neoantigens. *Genome Med* 2016;8:11.
- 21 Szolek A, Schubert B, Mohr C, *et al.* OptiType: precision HLA typing from next-generation sequencing data. *Bioinformatics* 2014;30:3310–6.
- 22 Hodi FS, Ballinger M, Lyons B, *et al.* Immune-Modified response evaluation criteria in solid tumors (imRECIST): refining guidelines to assess the clinical benefit of cancer immunotherapy. *J Clin Oncol* 2018;36:850–8.
- 23 Zacharakis N, Chinnasamy H, Black M, *et al.* Immune recognition of somatic mutations leading to complete durable regression in metastatic breast cancer. *Nat Med* 2018;24:724–30.
- 24 Broutier L, Mastrogiovanni G, Versteegen MM, *et al.* Human primary liver cancer-derived organoid cultures for disease modeling and drug screening. *Nat Med* 2017;23:1424–35.
- 25 Hida N, Maeda Y, Katagiri K, *et al.* A simple culture protocol to detect peptide-specific cytotoxic T lymphocyte precursors in the circulation. *Cancer Immunol Immunother* 2002;51:219–28.
- 26 Noguchi M, Sasada T, Itoh K. Personalized peptide vaccination: a new approach for advanced cancer as therapeutic cancer vaccine. *Cancer Immunol Immunother* 2013;62:919–29.
- 27 Dudley ME, Yang JC, Sherry R, *et al.* Adoptive cell therapy for patients with metastatic melanoma: evaluation of intensive myeloablative chemoradiation preparative regimens. *J Clin Oncol* 2008;26:5233–9.
- 28 Sia D, Jiao Y, Martinez-Quetglas I, *et al.* Identification of an Immune-specific class of hepatocellular carcinoma, based on molecular features. *Gastroenterology* 2017;153:812–26.
- 29 Singal G, Miller PG, Agarwala V, *et al.* Association of patient characteristics and tumor genomics with clinical outcomes among patients with non-small cell lung cancer using a Clinicogenomic database. *JAMA* 2019;321:1391–9.
- 30 McGranahan N, Furness AJS, Rosenthal R, *et al.* Clonal neoantigens elicit T cell immunoreactivity and sensitivity to immune checkpoint blockade. *Science* 2016;351:1463–9.
- 31 Chan TA, Wolchok JD, Snyder A. Genetic basis for clinical response to CTLA-4 blockade in melanoma. *N Engl J Med* 2015;373:1984.
- 32 Hellmann MD, Nathanson T, Rizvi H, *et al.* Genomic features of response to combination immunotherapy in patients with advanced non-small-cell lung cancer. *Cancer Cell* 2018;33:843–52.
- 33 Antonioli L, Pacher P, Vizi ES, *et al.* CD39 and CD73 in immunity and inflammation. *Trends Mol Med* 2013;19:355–67.
- 34 Deaglio S, Dwyer KM, Gao W, *et al.* Adenosine generation catalyzed by CD39 and CD73 expressed on regulatory T cells mediates immune suppression. *J Exp Med* 2007;204:1257–65.
- 35 Canale FP, Ramello MC, Núñez N, *et al.* CD39 expression defines cell exhaustion in tumor-infiltrating CD8<sup>+</sup> T cells. *Cancer Res* 2018;78:115–28.
- 36 Pauken KE, Wherry EJ. Overcoming T cell exhaustion in infection and cancer. *Trends Immunol* 2015;36:265–76.
- 37 Linnemann C, van Buuren MM, Bies L, *et al.* High-throughput epitope discovery reveals frequent recognition of neo-antigens by CD4<sup>+</sup> T cells in human melanoma. *Nat Med* 2015;21:81–5.
- 38 Verdegaal EME, de Miranda NFCC, Visser M, *et al.* Neoantigen landscape dynamics during human melanoma-T cell interactions. *Nature* 2016;536:91–5.



Supplemental Table 1.

HAN-low patients' Data																
Patient ID	Sex	Age	Relapse	PS score	BCLCL stage	HCV/ HBV	Child-pugh	Cirrhosis	AFP(IU/ml)	Number of Tumors	Diameter of largest Tumor(mm)	MVI	Metastasis	Die=1; Live=0	OS ( month )	Future Treatments
HCC03	male	71	yes	0	B	HBV	A	no	362.8	1	37	no	no	1	97	TACE+sorafenib
HCC06	male	42	yes	0	C	HBV	A	no	730	multinodular	25	no	yes	1	40	TACE+apatinib+Nivolumab
HCC08	male	61	no	1	C	HBV	B	yes	32.44	3	77	yes	no	1	8	TACE+sorafenib
HCC09	male	49	no	0	B	HBV	A	yes	154.04	multinodular	99	no	no	1	9	TACE+Lenvatinib
HCC10	male	48	yes	1	C	HBV	A	yes	2598.25	multinodular	46	no	yes	1	43	TACE+sorafenib
HCC11	male	66	no	0	B	HBV	A	yes	56316.29	multinodular	88	no	no	0	15	TACE+Lenvatinib+Pembrolizumab
HCC18	male	45	no	1	C	HBV	A	yes	54581.94	multinodular	107	yes	no	0	18	TACE+sorafenib
HCC19	male	73	no	0	A	HBV	A	no	1.61	2	78	yes	no	0	18	TACE+Lenvatinib+Pembrolizumab
HCC20	male	50	yes	1	C	HBV	C	yes	5604.17	multinodular	135	yes	yes	1	6	TACE+sorafenib+Nivolumab
HCC21	male	41	no	0	B	HBV	A	no	2113.1	multinodular	77	no	no	0	12	TACE+sorafenib
HCC23	male	40	no	1	C	HBV	A	yes	7360.23	multinodular	168	yes	yes	0	14	TACE+Lenvatinib
HCC25	male	46	no	0	B	HBV	A	yes	466032.08	multinodular	115	no	no	0	14	TACE+Lenvatinib+Pembrolizumab
HCC27	male	51	no	0	C	HBV	A	yes	9.71	multinodular	8.5	yes	no	0	14	TACE+Lenvatinib
HCC28	male	37	no	0	B	HBV	A	yes	3.26	1	91	no	no	0	20	TACE+sorafenib
HCC32	male	56	no	1	C	HBV	B	no	7462.8	multinodular	45	no	yes	1	3	TACE+sorafenib
HCC35	male	37	no	1	C	HBV	A	yes	7922.94	multinodular	93	yes	no	1	13	TACE+Lenvatinib+Pembrolizumab
HCC37	male	37	no	1	C	HBV	B	yes	2108.28	multinodular	24	yes	yes	1	5	TACE+sorafenib
HCC38	male	42	no	1	C	HBV	A	yes	16774.6	multinodular	130	yes	no	1	8	TACE+sorafenib
HCC41	male	59	no	1	C	HBV	B	yes	56393.51	multinodular	105	yes	no	1	5	TACE+sorafenib+Nivolumab
HCC42	male	83	no	0	A	No	A	no	42.5	1	36	no	no	0	9	TACE+sorafenib
HCC43	male	54	no	0	B	HBV	A	yes	5289.79	1	102	no	yes	0	8	TACE+sorafenib
HCC44	male	39	no	0	C	HBV	A	no	4.96	1	129	yes	no	0	32	TACE+sorafenib
HCC46	male	51	no	1	C	HBV	B	yes	3080.25	1	53	yes	no	1	4	TACE+sorafenib
HCC48	male	56	yes	0	C	HBV	A	no	2.72	multinodular	33	no	yes	0	71	TACE+sorafenib+Nivolumab
HCC50	male	55	yes	1	C	HBV	B	yes	6711.69	multinodular	82	yes	yes	1	62	TACE+sorafenib
HCC53	female	31	yes	0	A	HBV	A	no	1317.36	1	114	yes	yes	0	6	TACE+sorafenib
HCC55	male	46	no	1	C	HBV	B	yes	118.82	multinodular	184	no	no	0	6	TACE+sorafenib
HCC56	male	46	yes	0	B	HBV	A	yes	2.07	multinodular	36	no	no	0	6	TACE+sorafenib
HAN-high patients' Data																
Patient ID	Sex	Age	Relapse	PS score	BCLCL stage	HCV/ HBV	Child-pugh	Cirrhosis	AFP(IU/ml)	Number of Tumors	Diameter of largest Tumor(mm)	MVI	Metastasis	Die=1; Live=0	OS ( month )	Future Treatments

HCC01	male	49	no	0	C	HBV	A	no	30.13	2	128	no	no	0	40	TACE+sorafenib+Nivolumab
HCC02	male	42	no	0	B	HBV	A	yes	12523.75	2	120	no	no	0	15	TACE+apatinib
HCC04	male	51	yes	0	B	HBV	A	yes	312.79	1	47	no	no	0	36	TACE+apatinib
HCC05	male	42	no	0	C	HBV	A	no	33.53	multinodular	92	yes	no	0	12	TACE+sorafenib
HCC07	female	61	no	0	B	HBV	A	no	2.64	3	35	yes	no	0	64	TACE+apatinib
HCC12	male	70	no	0	B	HBV	A	yes	90.66	multinodular	98	no	no	0	12	TACE+Lenvatinib+Pembrolizumab
HCC13	male	47	no	1	C	HBV	A	no	1.61	multinodular	69	yes	yes	1	17	TACE+Lenvatinib
HCC14	male	55	yes	0	C	HBV	A	yes	1.67	3	79	yes	yes	0	60	TACE+Lenvatinib
HCC15	male	60	yes	0	C	HBV	A	yes	39.82	multinodular	20	yes	no	1	143	TACE+Lenvatinib+Pembrolizumab
HCC16	male	71	yes	1	C	HBV	A	yes	122.77	multinodular	15	yes	yes	1	50	TACE+sorafenib+Nivolumab
HCC17	male	49	no	0	A	HBV	A	yes	4.53	3	22.6	no	no	0	15	TACE+sorafenib
HCC22	male	78	yes	1	C	HBV	A	no	32.8	multinodular	58	yes	no	1	29	TACE+sorafenib+Nivolumab
HCC24	male	65	no	1	C	HBV	A	yes	4316.08	2	106	yes	yes	1	15	TACE+Lenvatinib
HCC26	male	49	yes	0	C	HBV	A	yes	204.58	2	83	yes	no	0	56	TACE+Lenvatinib
HCC29	male	54	no	1	C	HBV	B	no	1.58	multinodular	78	yes	yes	1	6	TACE+sorafenib
HCC30	male	72	no	0	B	HBV	A	yes	11.83	multinodular	27	no	yes	0	14	TACE+sorafenib
HCC31	male	35	no	1	B	HBV	A	yes	1741.23	2	62	no	no	1	39	TACE+sorafenib
HCC33	male	60	no	1	C	HBV	A	yes	1762.4	1	80	yes	no	1	9	TACE+Lenvatinib
HCC34	male	55	no	0	B	HBV	A	no	306.8	1	48	no	no	0	11	TACE+sorafenib
HCC36	male	56	no	0	C	HBV	A	no	9470.9	multinodular	98	yes	yes	0	10	TACE+Lenvatinib
HCC39	male	65	yes	0	A	HBV	A	yes	7.16	3	61	yes	no	0	61	TACE+Lenvatinib
HCC40	male	59	yes	0	C	HBV	A	No	423.67	multinodular	68	no	no	0	111	TACE+sorafenib+Nivolumab
HCC45	male	69	no	0	B	HBV	A	no	640.15	2	109	no	no	0	8	TACE+sorafenib
HCC47	male	59	yes	0	B	HBV	A	no	3034.3	multinodular	53	no	no	0	72	TACE+sorafenib+Nivolumab
HCC49	male	55	yes	1	C	HBV	A	no	2.83	multinodular	28.3	no	yes	0	78	TACE+sorafenib
HCC51	male	46	yes	0	A	HBV	A	no	102.2	1	56	no	no	0	23	TACE+sorafenib+Nivolumab
HCC52	male	52	no	1	C	HBV	B	yes	1205.17	multinodular	165	yes	yes	0	7	TACE+sorafenib
HCC54	male	40	no	1	C	HBV	B	yes	67.33	multinodular	13	yes	yes	0	6	TACE+sorafenib

Supplemental Table 1. The clinical data of all 56 patients of HAN-high/low groups.

Clinical data was obtained according to the clinical charts and Imaging information of the patients and then divided into HAN-high/low groups. PS score: Performance status score; AFP:serum alpha-fetoprotein; BCLC, Barcelona Clinic Liver Cancer staging system; Child-pugh: Child-pugh score for liver function; MVI: Microvascular invasion; OS: overall survival. Treatments of all the patients were after needle biopsy.

Patient data highlighted in red and blue indicated the six representative patients selected in each group for TILs and autologous tumors organoids killing assay. Patient data highlighted in red indicated three candidate patients selected for specific high-affinity peptide identification assay.

Supplemental Table 2.

Supplemental HAN-low patients Data															
Patient	Sex	Age	Relapse	PS score	BCLCL stage	HCV/ HBV	Child-pugh	Cirrhosis	AFP(IU/ml)	Number of Tumors	Diameter of largest Tumor(mm)	MVI	Metastasis	Treatment afterwards	HAN Value
sHCC-01	male	62	no	1	B	HBV	A	yes	5404.55	multinodular	122	yes	no	operation	7
sHCC-02	female	62	no	0	B	No	B	no	1991.59	1	144	yes	no	operation	11
sHCC-03	male	49	no	0	B	HBV	A	no	43805.47	1	77	no	no	operation	12
sHCC-04	male	45	no	0	A	HBV	A	no	4.9	2	19	no	no	operation	11
sHCC-05	male	56	yes	1	B	HBV	A	yes	1209.91	1	77	yes	no	operation	8
sHCC-06	male	52	no	0	B	HBV	A	no	1.74	1	159	no	no	operation	11
Supplemental HAN-high patients Data															
Patient	Sex	Age	Relapse	PS score	BCLCL stage	HCV/ HBV	Child-pugh	Cirrhosis	AFP(IU/ml)	Number of Tumors	Diameter of largest Tumor(mm)	MVI	Metastasis	Treatment afterwards	HAN value
sHCC-07	male	67	no	0	B	HBV	A	yes	68238.12	multinodular	87	yes	no	operation	17
sHCC-08	male	62	no	0	B	HBV	A	yes	195.84	1	82	no	no	operation	16
sHCC-09	male	52	no	1	B	HBV	A	no	15.3	1	90	no	no	operation	19
sHCC-10	male	64	no	1	B	No	A	no	3.39	1	62	no	no	operation	38
sHCC-11	male	60	no	0	B	HBV	A	no	118.68	1	70	no	no	operation	22
sHCC-12	male	56	no	0	A	HBV	A	no	3.87	1	54	no	no	operation	26

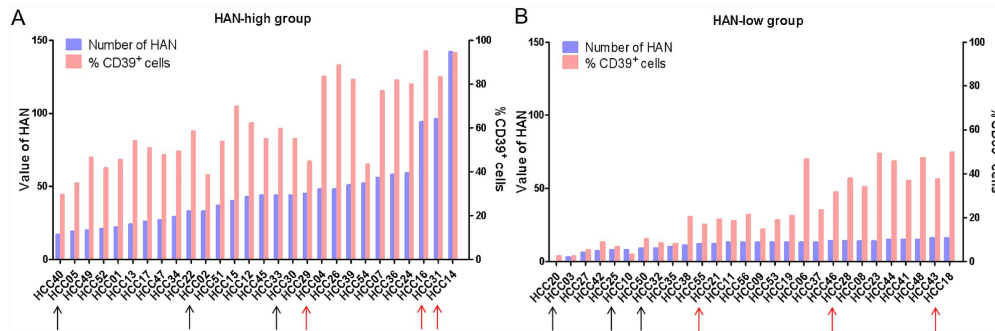
Supplemental Table 2. The clinical data of 12 patients of HAN-high/low groups treated with surgical resection.

Clinical data was obtained according to the clinical charts and Imaging information of the patients and then divided into HAN-high/low groups. PS score: Performance status score; AFP:serum alpha-fetoprotein; BCLC, Barcelona Clinic Liver Cancer staging system; Child-pugh: Child-pugh score for liver function; MVI: Microvascular invasion. All patients were taken WES sequence and HAN analysis.



1

## Supplemental Figures and legends



2

### 3 Supplemental Figure 1

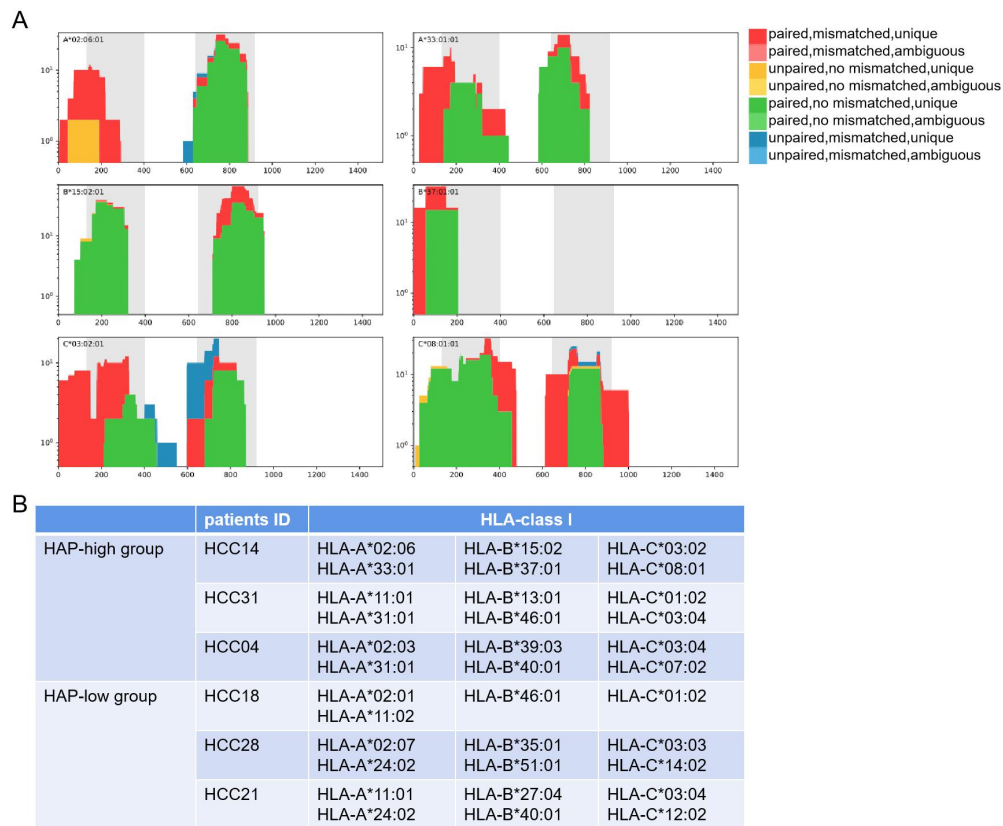
4 Summary of the frequency of CD39<sup>+</sup>CD8<sup>+</sup> TILs and value of HAN for all the 56 HCC

5 patients. (A-B) Red bars represented the frequency of CD39<sup>+</sup>CD8<sup>+</sup> TILs and blue bars

6 represented the value of HAN. Arrows indicated the six representative patients

7 selected for TILs and autologous tumors organoids killing assay. Red arrows indicated

8 three candidate patients selected for specific high affinity peptide identification assay.



9

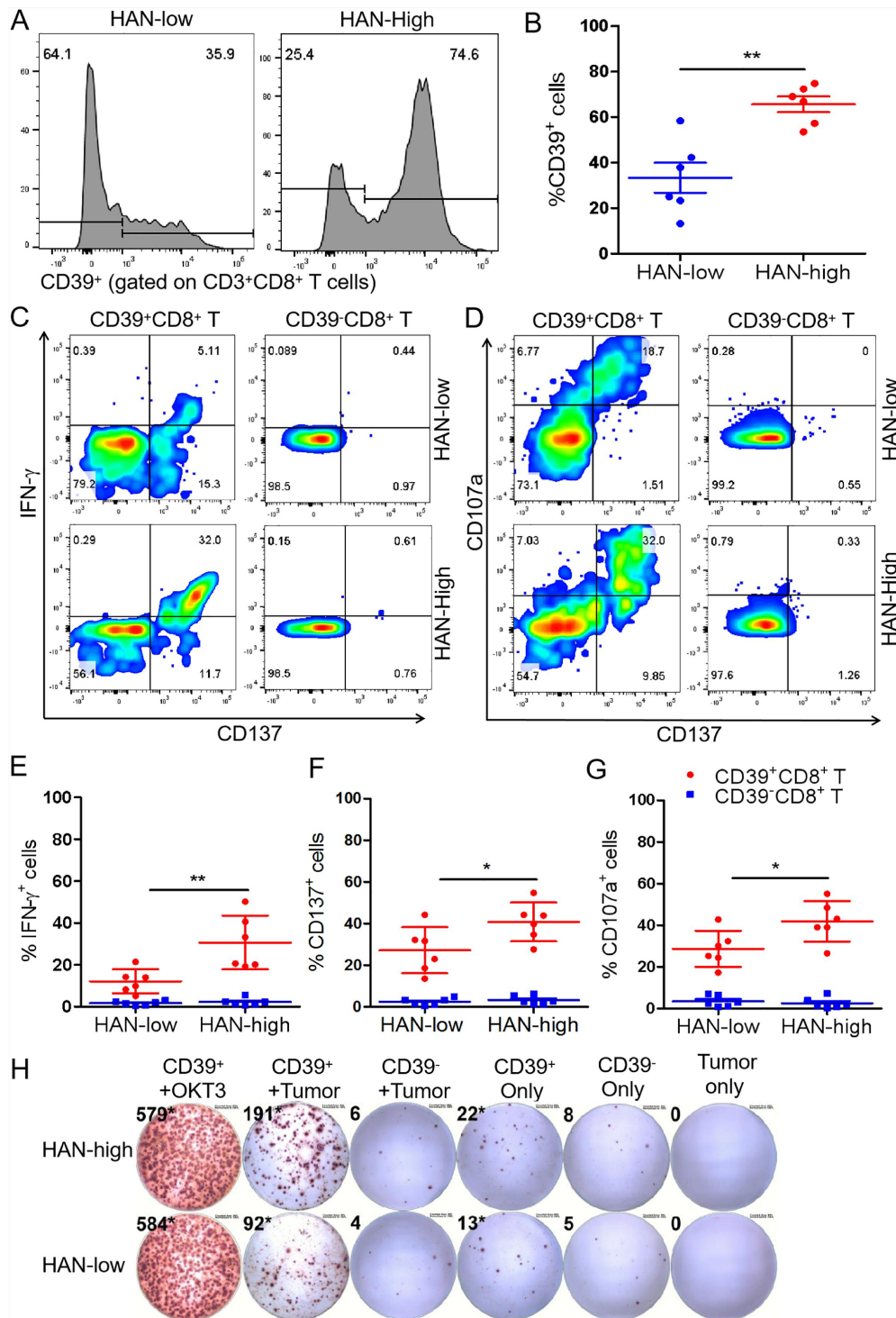
10 **Supplemental Figure 2**

11 HLA alleles Analysis by OptiType(v1.3.3) were shown for six candidate patients. (A)

12 The coverage plot of the HLA alleles for representative patient HCC14 analyzed by

13 OptiType were shown. Listed HLA alleles were with high expression abundance.

14 (B) Summary HLA alleles of all the six candidate patients were shown in this table.



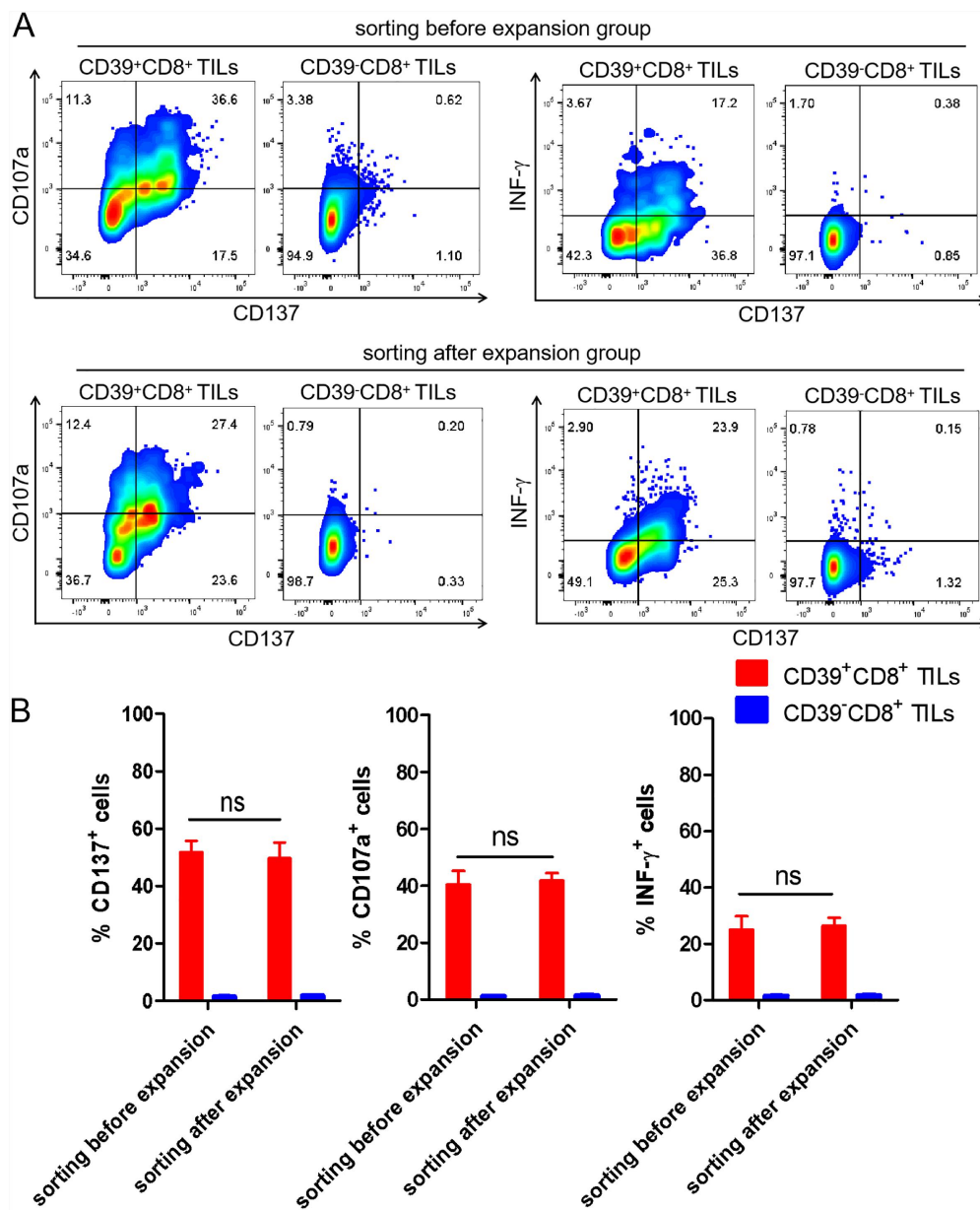
15

16 **Supplemental Figure 3**

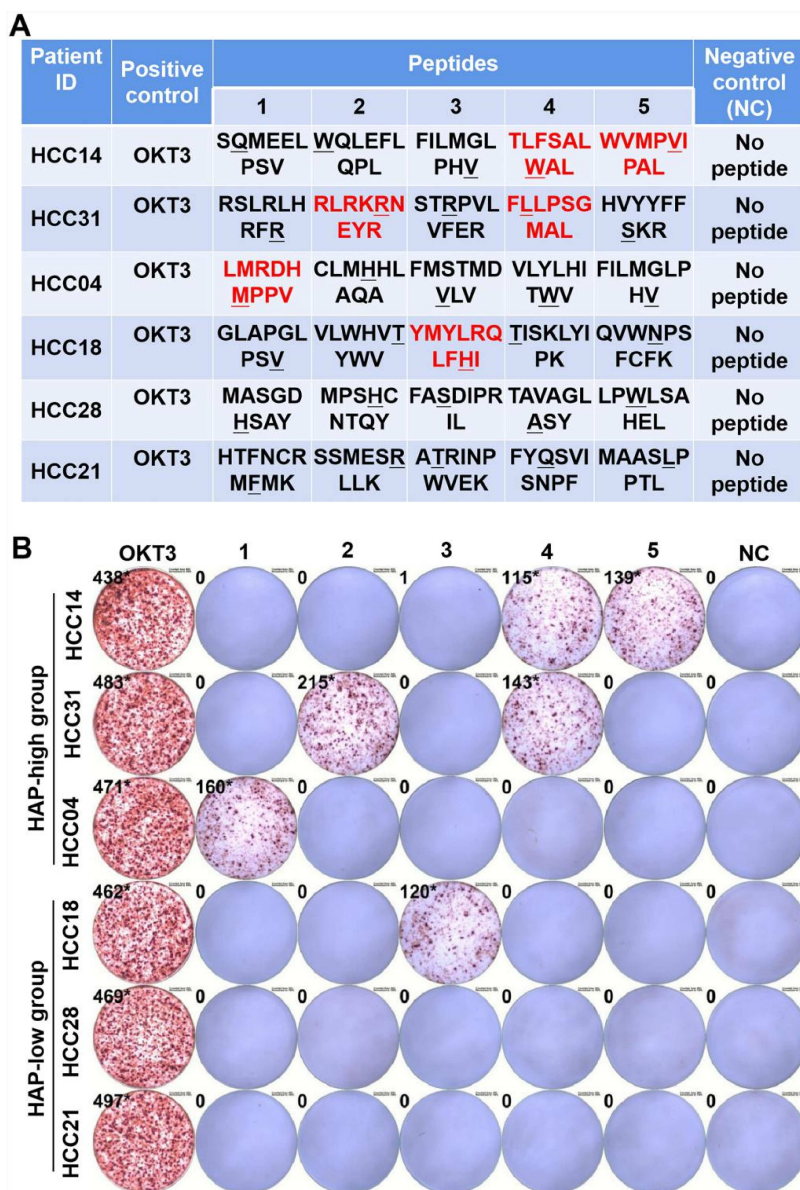
17 CD39 and effector molecules expressed on TILs from surgically removed HCC fresh

18 tumor samples. (A-B) The frequency of CD39<sup>+</sup>CD8<sup>+</sup> T cells in each group was  
19 detected by flow cytometry. (C-G)The expression of IFN- $\gamma$ , CD107a and CD137 on  
20 CD39<sup>+</sup>CD8<sup>+</sup> T cells was detected by flow cytometry. The dots represent different  
21 patients. Data are presented as mean  $\pm$  SEM (n=6), \* $P$  < 0.05, \*\* $P$  < 0.01.(H) CD39<sup>+</sup>/  
22 CD8<sup>+</sup> TILs were respectively sorted from surgically removed fresh tumor sample and  
23 co-cultured with or without (TILs only) autologous tumor cells, then the IFN- $\gamma$   
24 secretion was investigated by ELISPOT after 24 hours. OKT3 was used as positive  
25 control.





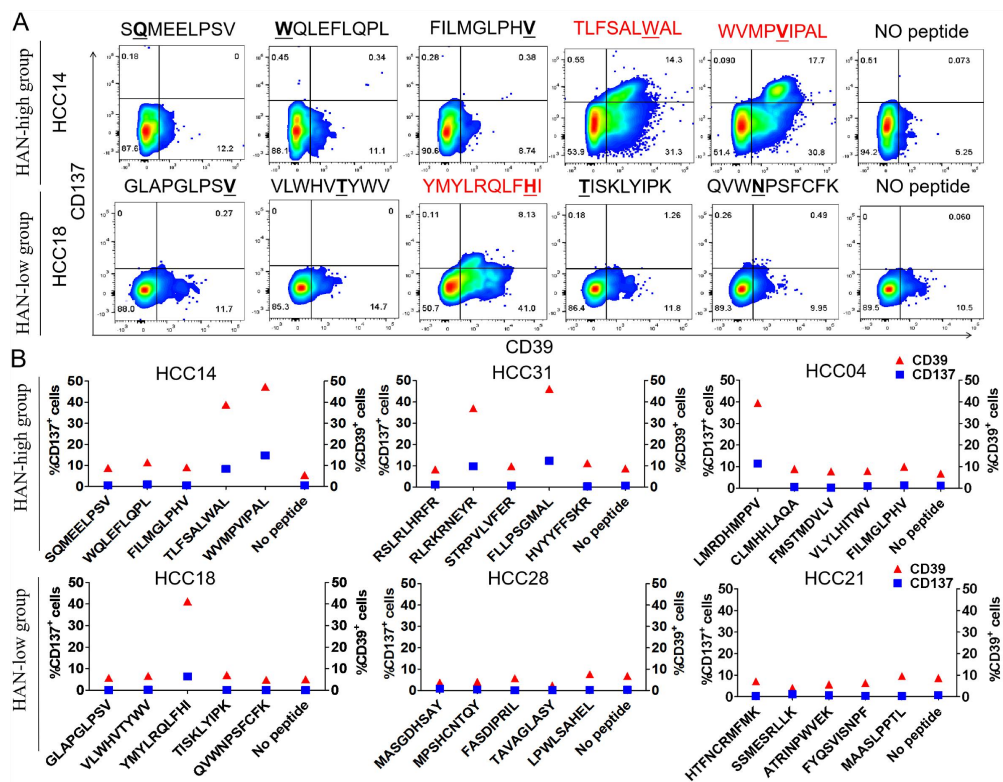
33 one was the sorting after expansion group which TILs were expanded first for 14 days  
 34 and then sorted by the marker of CD39. At day 14, TILs of each group was  
 35 co-cultured with tumor cells, and then the function of CD39<sup>±</sup> subsets was assessed by  
 36 flow cytometry with intracellular staining of IFN- $\gamma$ , CD107a and CD137. (B)  
 37 Summary of the frequency of IFN- $\gamma$ , CD107a and CD137 positive was shown.



38

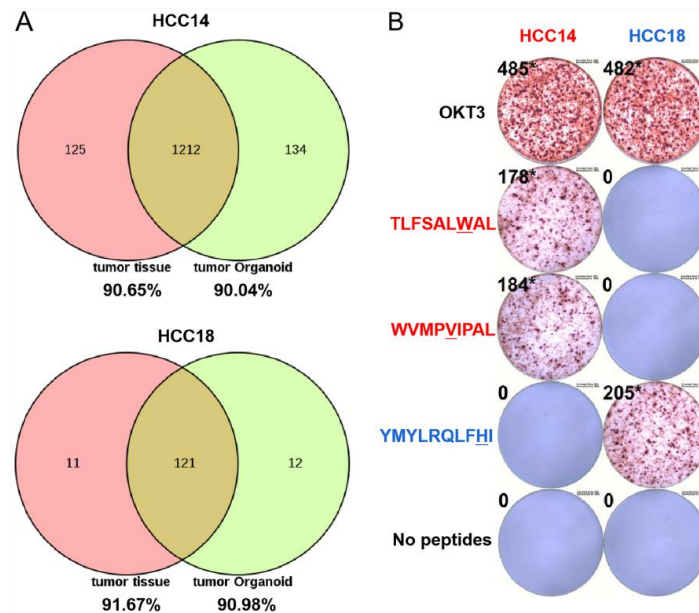
39 **Supplemental Figure 5**

40 Identification of personalized neoantigens for 6 patients. (A-B) Autologous PBMCs  
 41 were stimulated with top five candidate peptides for 10 days, after which autologous  
 42 tumor organoid from candidate patient was added to activate T-cell specific antigen  
 43 response 24h before IFN- $\gamma$  detection by ELISPOT assays. OKT3 was used as positive  
 44 control, and no-peptide stimulation was tested as negative control.

45 **Supplemental Figure 6**

47 Expression of CD137 and CD39 of tumor-reactive CD39<sup>+</sup>CD8<sup>+</sup> T cells by stimulation  
 48 with candidate HANs from PBMCs. (A) Flow cytometry plots gated on CD8<sup>+</sup> T cells  
 49 to analyze T cell effector sensitivity against tumor organoids by CD137 and CD39  
 50 up-regulation. (B) Summary of the frequency of CD39<sup>+</sup> or CD137<sup>+</sup> T cells was shown

51 for all the six representative patients.

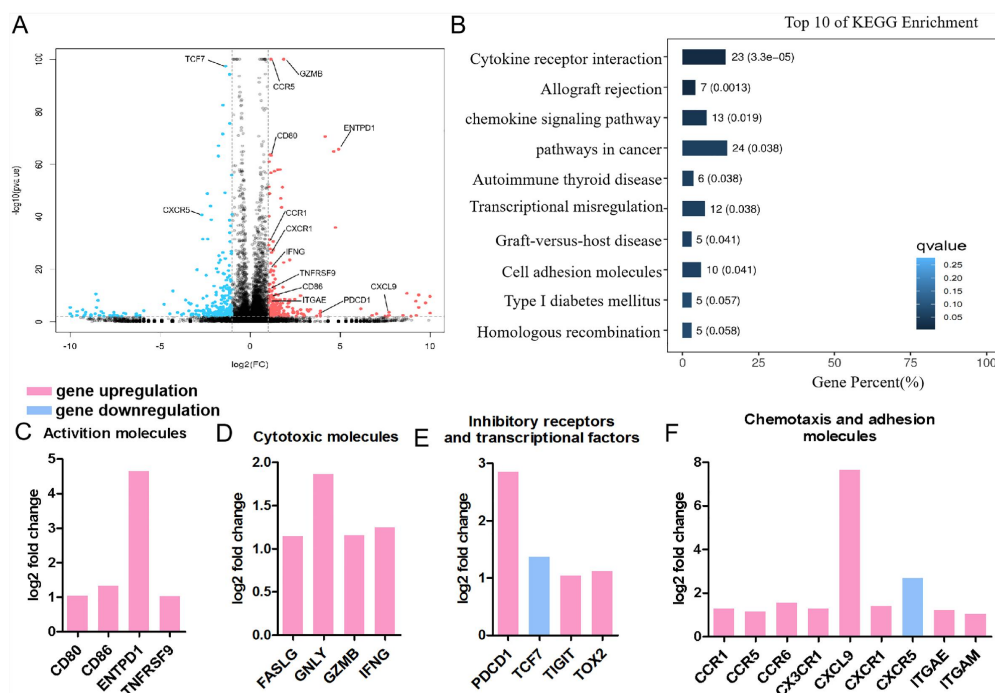


52

### 53 Supplemental Figure 7

54 Allogeneic positive peptides couldn't induce IFN- $\gamma$  release for autologous tumor  
 55 organoid killing. (A) Venn diagrams illustrate the number of somatic non-synonymous  
 56 mutations present in each tumor tissue and their derivative HCC organoids. The  
 57 similarity of mutation from tumor tissue and organoid was greater than 90%. (B)  
 58 Autologous PBMCs from candidate patients were stimulated with autologous peptides  
 59 (marked by the same color) and allogeneic peptides (marked by the different color)  
 60 for 10 days, after which autologous tumor organoids from candidate patient was  
 61 added to activate T-cell specific antigen response 24h before IFN- $\gamma$  detection by  
 62 ELISPOT assays. OKT3 was used as positive control, and no-peptide stimulation was  
 63 tested as negative control.





64

65 **Supplemental Figure 8**

66 RNA-seq data of CD39<sup>+</sup>-CD8<sup>+</sup> T cells stimulated by HAN peptide. PBMCs were  
 67 stimulated by autologous HANs for 10 days and then co-cultured with autologous  
 68 tumor organoids for 24h. After which CD39<sup>+</sup>-CD8<sup>+</sup> T cells were sorted by FACS for  
 69 following RNA-seq assay. (A) Volcano graph revealed the difference of genes  
 70 expression analyzed by RNA-seq between CD39<sup>+</sup>-CD8<sup>+</sup> T cells after stimulation by  
 71 HAN peptide (log<sub>2</sub>-transformed). The dashed line identified the differently expressed  
 72 genes when using a P value <0.05. (B) KEGG enrichment demonstrated the  
 73 significant enrichment of top 10 pathways using a P/Q value. (C-F) Bar plots  
 74 indicated the RNA-seq expression of log<sub>2</sub> fold change of major up-regulated and  
 75 down-regulated genes in CD39<sup>+</sup>CD8<sup>+</sup> T cells compared to CD39<sup>-</sup>CD8<sup>+</sup> T cells (P  
 76 <0.05). Pink bars represented up-regulation and blue bars represented  
 77 down-regulation.